In presenting the dissertation as a partial fulfillment of the requirements for an advanced degree from the Georgia Institute of Technology, I agree that the Library of the Institute shall make it available for inspection and circulation in accordance with its regulations governing materials of this type. I agree that permission to copy from, or to publish from, this dissertation may be granted by the professor under whose direction it was written, or, in his absence, by the Dean of the Graduate Division when such copying or publication is solely for scholarly purposes and does not involve potential financial gain. It is understood that any copying from, or publication of, this dissertation which involves potential financial gain will not be allowed without written permission.

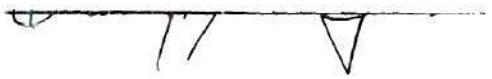

7/25/68

# A LOW DIFFERENTIAL PRESSURE TRANSDUCER

A THESIS

Presented to

The Faculty of the Division of Graduate

Studies and Research

by

Oscar Javier Montemayor

In Partial Fulfillment

of the Requirements for the Degree

Master of Science in Mechanical Engineering

Georgia Institute of Technology

December, 1970

A LOW DIFFERENTIAL PRESSURE TRANSDUCER

Approved:

[redacted]

Date approved by Chairman: December 14, 1970

# ACKNOWLEDGMENTS

The author would like to express his grateful appreciation to Dr. Prateen V. Desai, thesis adviser, for his hard work and expert guidance during both the research and written parts of this thesis. Dr. James H. Rust and Dr. Ward O. Winer, members of the reading committee, contributed suggestions which helped to clarify some ideas expressed in this thesis.

The author is indebted to Dr. Stothe P. Kezios and to Dr. Pandeli Durbetaki for granting him a teaching assistantship. Messrs. R. G. Grim, B. L. Wallace, and H. J. Carr gave advice and assistance in the fabrication of the transducer. Mr. Neil Martin gave technical help with the electronic instrumentation.

The author is also indebted to Mr. and Mrs. Theodore L. Garby for their help and encouragement at the right times throughout these graduate studies.

This thesis is dedicated to the parents of the author and to Miss Gloria Garcia for their concern, love, and continued encouragement in this part of his life.

TABLE OF CONTENTS

# LIST OF TABLES

# LIST OF ILLUSTRATIONS

LIST OF ILLUSTRATIONS (Concluded)

## SUMMARY

Investigation of the dynamics of low density and low total pressure internal flows often necessitates the use of precise pressure instrumentation with adequate frequency response. Commercially available transducers for low density investigations are usually cumbersome for static work and limited in application for dynamic studies.

This thesis undertakes an investigation of a new research tool for the measurement of both static and dynamic differential pressures in the range of one thousandths of a pound per square inch.

The basic design involves the use of a proximity sensor consisting of a vibrating Mylar membrane, a light-beam-carrier bundle of fibers, a light source, a photocell, and a readout system.

A dynamic analysis of the pressure fluctuations in an isothermal chamber has been presented which yields expressions for predicted pressure response. A lumped parameter model has been used to describe the process. The analysis takes into account the change of volume due to the vibrating membrane as well as the change of volume due to compressibility of the fluid.

A series of tests have been conducted to obtain the static as well as the dynamic characteristics of the test transducers. Finally, the experimental and theoretical results are compared.

# NOMENCLATURE

| | |
|---|---|
| $A$ | area of line |
| $C$ | perimeter of line |
| $E$ | elasticity modulus |
| $F$ | line shear-resistance constant |
| $G$ | integration function |
| $H$ | integration function |
| $J$ | constant |
| $K$ | constant |
| $K_1$ | constant |
| $K_2$ | constant |
| $L$ | length of the tube |
| $M_{cavity}$ | mass in the cavity |
| $P$ | transducer pressure |
| $P_a$ | input pressure |
| $P_w$ | sinusoidal pressure amplitude |
| $R$ | frictional resistance |
| $V$ | volume in the cavity |
| $dV_m$ | change of volume of the membrane |
| $W$ | total applied load |
| $a$ | sound speed |
| $f_r$ | membrane resonant frequency |
| $\ell$ | displacement of piston |

NOMENCLATURE (Concluded)

| | |
|---|---|
| $j$ | imaginary operator |
| $m$ | inverse of Poisson's ratio |
| $n$ | ratio of specific heats |
| $r$ | radial distance from the center of the membrane |
| $r_o$ | diaphragm radius |
| $s$ | Laplace operator |
| $t$ | thickness of membrane |
| $u$ | streamwise velocity in the line |
| $x$ | distance along the line |
| $y$ | deflection of the membrane |
| $y_{max}$ | deflection of the membrane at the center |

Greek Letters

| | |
|---|---|
| $\beta$ | bulk modulus of elasticity |
| $\phi$ | phase shift angle |
| $\xi$ | damping ratio |
| $\omega$ | frequency |
| $\omega_n$ | resonant frequency |
| $\sigma_r$ | radial stress |
| $\nu$ | Poisson's ratio |
| $\rho$ | density |
| $\mu$ | fluid viscosity |
| $\Delta$ | change of a variable |

# CHAPTER I

# INTRODUCTION

## General Problem of Low Pressure Measurements

The pressure exerted by a fluid is given in terms of force acting on a unit area. The measurement of pressure and vacuum has always been important in both continuous-processing industries as well as sophisticated research applications. In a great number of industrial and laboratory applications, it is often more important and easier to make precise measurement of pressure than it is to measure temperatures. The very rapid advance of low density technology has necessitated the development of newer and more sensitive pressure instrumentation.

Usually pressure is measured by transducing the force effect to a deflection or deviation through a transmission line and transducer chamber, together with either a gravitational or an elastic restraining element. The gravitational restraining type of element leads to various types of manometers. The elastic restraining elements generally have an electro-mechanical secondary element which converts the displacement of a membrane to an electric signal. The principal feature of these devices is the ease of amplification, control, transmission, and measurement of the response signals.

The range of pressures that can be measured by either of the preceding categories of instruments is rather variable. The simplest of the

manometers is the U-tube manometer. Pressure is applied in both or one leg of the U-tube giving a differential or gauge pressure and requires a reading of both legs. The well-type manometer requires reading of only a single leg. The well area is made large compared with that of the tube, thus the level of the manometer fluid in this area is displaced very little compared with that in the tube leg when pressure is applied. This small error is compensated by suitable distortion of the length scale. To increase sensitivity, the manometer leg may be tilted with respect to gravity, thus giving a greater change of liquid column along the tube for a given vertical height change. Such an inclined manometer can give a reading to the accuracy of a hundredths of an inch of water. Errors in these manometer-type of transducers may be due to the variation of density with temperature, the gravity not being corrected for the local value, or due to the difficulty in reading the height due to the meniscus formed by capillarity. Range can be extended by use of special optical sight glasses, such as the cathetometer. When mercury is the manometer fluid, variable reluctance pick-up may be used to accurately sense the fluid height. In the case that the manometer fluid is not mercury, special metal floats may also afford such a convenience with less dense fluids which are non-conductive. Electrical pick-ups reduce human errors and produce a signal which can be utilized for control purposes and may give a resolution of five thousandths of an inch.

In several applications it becomes paramount to obtain very small, yet precise, differential pressure measurements. The micromanometer which is a variation of the inclined manometer has a hairline as a

reference point and possesses a vernier scale for accurate null balance. If alcohol is used as the fluid in such a micromanometer, a resolution of one millionth of a pound per square inch can be obtained. In an air micromanometer, the unknown pressure is equalized with a pressure which is generated by two rotating disks. When the pressures are equal, oil level falls vertically. It gives a reading of two thousandths of an inch of water with one percent of uncertainty. It may be noted that, regardless of the accuracy of measurement obtained by these devices, they are still rather severely limited for dynamic measurements.

On the other hand, transducers with elastic restraining elements have usually found applicability both in the low pressure range as well as dynamic measurements. These devices can be further divided into two categories, depending on whether the secondary element is passive or active. An active element is one which generates its own potential. Conversely, the passive type of secondary element needs an imposed potential for its operation. In the active-secondary-element category there are only the piezoelectric crystal transducers. Pressure transducers of a passive-secondary-element type can be subdivided into several categories, depending on their principle of operation. Typically, these are the capacitive type, the strain gage type, the potentiometer, the linear variable differential transformer, the inductive variety, or the electrokinetic potential type.

Piezoelectric crystals are high output impedance devices, requiring high input impedance amplifiers with sufficiently low leak, which makes static measurements rather difficult. A piezoelectric pressure transducer

is usually restricted to dynamic measurements. The deflection of a diaphragm under pressure may also be sensed by measuring the capacitive variation; this pick-up, however, has inherently low sensitivity and special care must be exerted in the construction of the read-out circuitry. Strain gages measure the local strain of the diaphragm, which, in turn, may be related to the diaphragm deflection and pressure differential which causes it. These gages are very sensitive but are relatively limited in dynamic response. Pressure pick ups using resistive potentiometers are not intended for measurements of very fast pressure changes because they require a large internal volume and volume changes, as well as a finite operating life. A linear variable differential transformer permits measurements of pressure as low as thirty five millionths of a pound per square inch. An inductive type of transducer as well as the linear variable differential transformer are both usually suited for static and dynamic work. The latter has the capability of replacable diaphragms that the former does not have. For these transducers the read-out circuitry is complicated. An electrokinetic potential type of device uses a fluid flowing through a porous disk to generate an electric potential, but it is suitable only for dynamic measurements.

## Purpose and Scope of the Present Work

From the preceding discussion, it seems reasonable to attempt an investigation of either a new principle of operation for low pressure measurement or, at least, a new technique for these measurements. Several

constraints that are imposed on the instrument are as follows: fabrication of the transducer must be simple and compact; it must be suitable for low pressure measurements, both differential and absolute; the range of such a new transducer must be for pressures of the order of one thousandths of a pound per square inch or lower; it must have an acceptable dynamic response; it should put out a controlled output; the overall measurement system should be relatively simple.

The basic principle of operation of the pressure transducer selected in this investigation is the linear deflection of a Mylar film in the vicinity of a proximity sensor which measures the displacement of the membrane and relates it to the pressure differential. The proximity sensor consists of a light-beam-carrier bundle of fibers placed in front of the membrane which carries light from a light source to the membrane surface and collects the reflected light and transmits it to a photocell. The amount of reflected light varies with the displacement of the membrane and thus the output of the photocell is related to the applied pressure differential.

The distinguishing features of this transducer from commercially available units are its compactness and the lack of complex circuitry associated with the measurements. An output transistorized amplifier operating in conjunction with a photo transceiver from a dry cell battery source will satisfy the basic requirements. The transducer, when placed in proximity to the membrane, will produce an output that may be transmitted with fiber optics which is free from the effects of electromagnetic and electrostatic radiation problems so frequently encountered in

industrial applications today. Dynamic and static measurements may be conducted with the device and it is adaptable to various pressure ranges by a mere change of the sensing membrane.

The intent of this study is to investigate the feasibility of developing such a pressure transducer, by first developing an analytical model, followed by static and dynamic experimentation.

# CHAPTER II

## TRANSDUCER DESIGN AND ANALYSIS

### Preliminary Design Considerations

Consider a light beam passing through a bundle of optical fibers toward a flat surface held normal to the fibers. This bundle of fibers has characteristics such that bundle A transmits light from a light source and bundle B transmits back the light reflected by the work surface to a photocell, as shown in Figure 1. Bundles A and B are bonded together at one end and separated at the other end, but are free to flex through the remainder of their length. The distribution geometry of the fibers of bundles A and B at the common end is random (can be hemispheric or concentric). The fibers can be fabricated from glass which can withstand a temperature as high as one thousand degrees Farenheit, or from synthetic fibers which are very flexible and which possess excellent transmission characteristics, both in the visible spectrum as well as in the infrared band. These fibers are non-contacting type of elements, and as such they do not add weight or absorb power from the observed object. Magnetic or electrostatic disturbances do not affect the operation of the fiber optics, neither is there any need for electrical grounding. The reflected light beam from the plate is carried back through the bundle B as shown in Figure 1. A photocell at the end received the light reflected by the surface. The reflected light intensity is a function of the

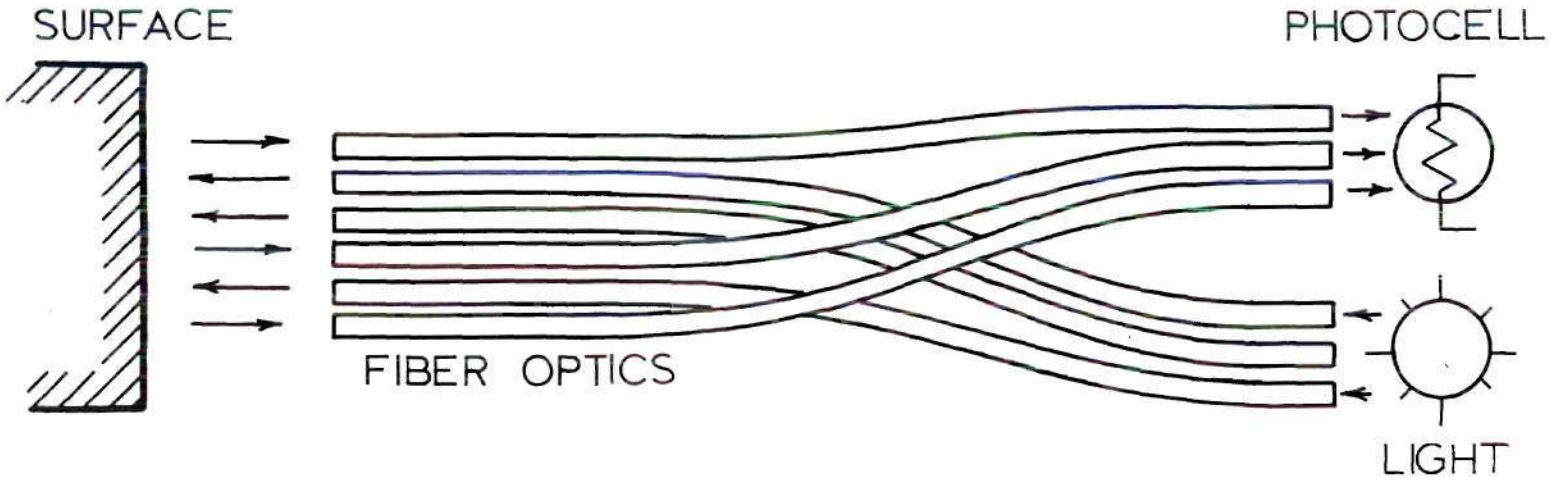


Figure 1. Fiber Optics Arrangement

distance between the flat surface and the fiber optics. Change of distance causes variation in the light intensity received by the photocell. The photocell output, in turn, is proportional to the intensity of light received, which may be related to the distance between the fibers and the flat surface. If the surface proximity decreases the output of the photocell increases, and vice versa.

When the reflecting surface consists of a circular diaphragm or membrane held fixed along its circumference, and when it vibrates in response to a uniformly distributed fluid force, the proximity of the membrane is reflected in the amount of light recovered by the photocell, whose output is then a measure of the deflection of the membrane. The deflection of the membrane varies directly with the fluid force applied; therefore, the output of the photocell is dependent upon the fluid force. If the photocell output is amplified by an electronic circuit and if the output is plotted versus distance, calibration curves may be obtained to relate the proximity of the surface to the amplified photocell output. The intensity of the light is kept in agreement with the reflectivity of the material by selecting higher light intensity for surfaces with low reflectivity. The light source with intensity control, the photocell, the fiber optics, and the amplifier are built in within an apparatus called a fotonic sensor. The current and voltage characteristic curves for the fotonic sensor are shown in Figures 2 and 3, respectively.

It may be noted here that the curves are linear only in limited ranges of gap distances. The first linear range has high sensitivity while the second one has less sensitivity, the latter having a wider linear

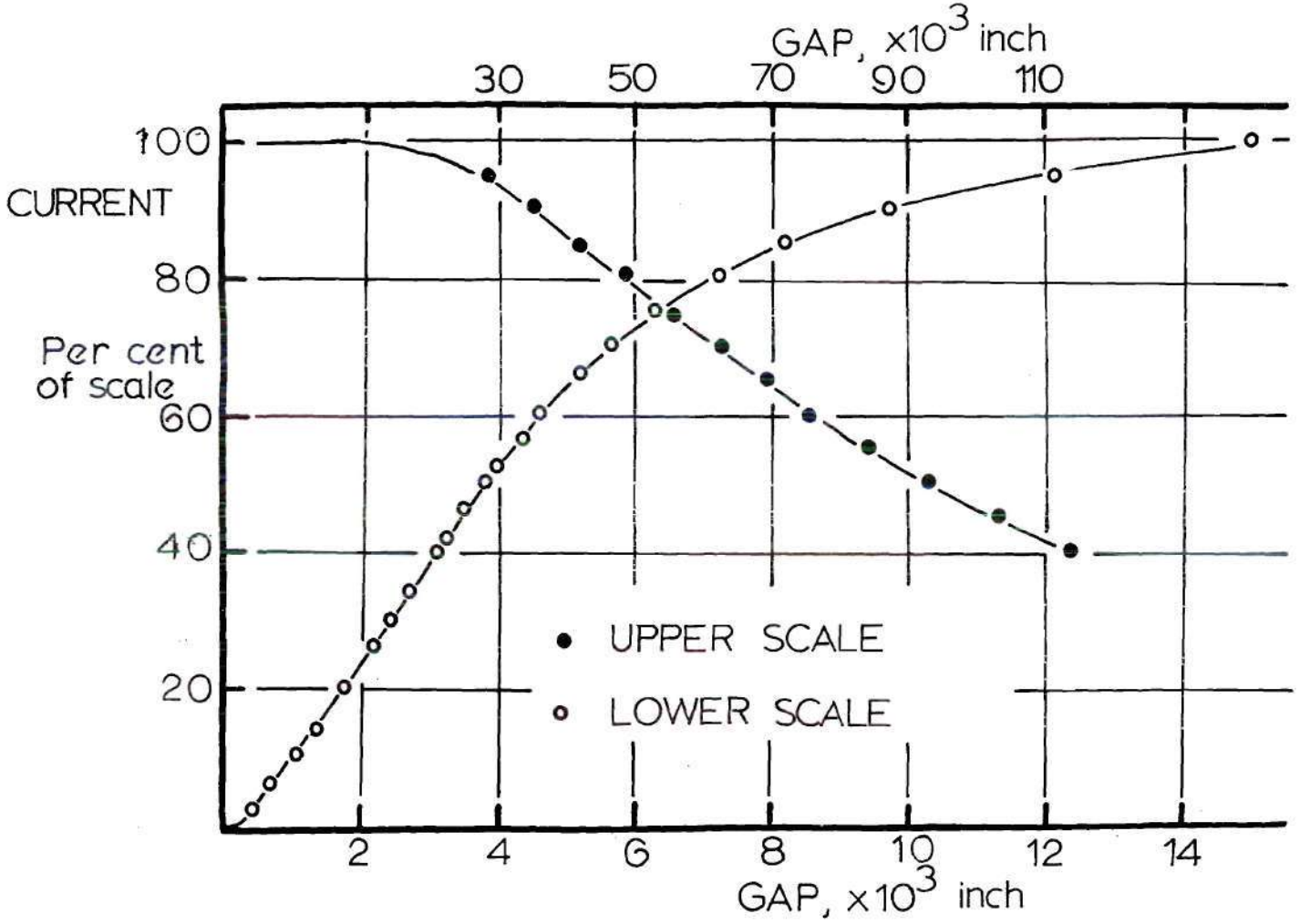


Figure 2. Current Calibration Curve for Fotonic Sensor

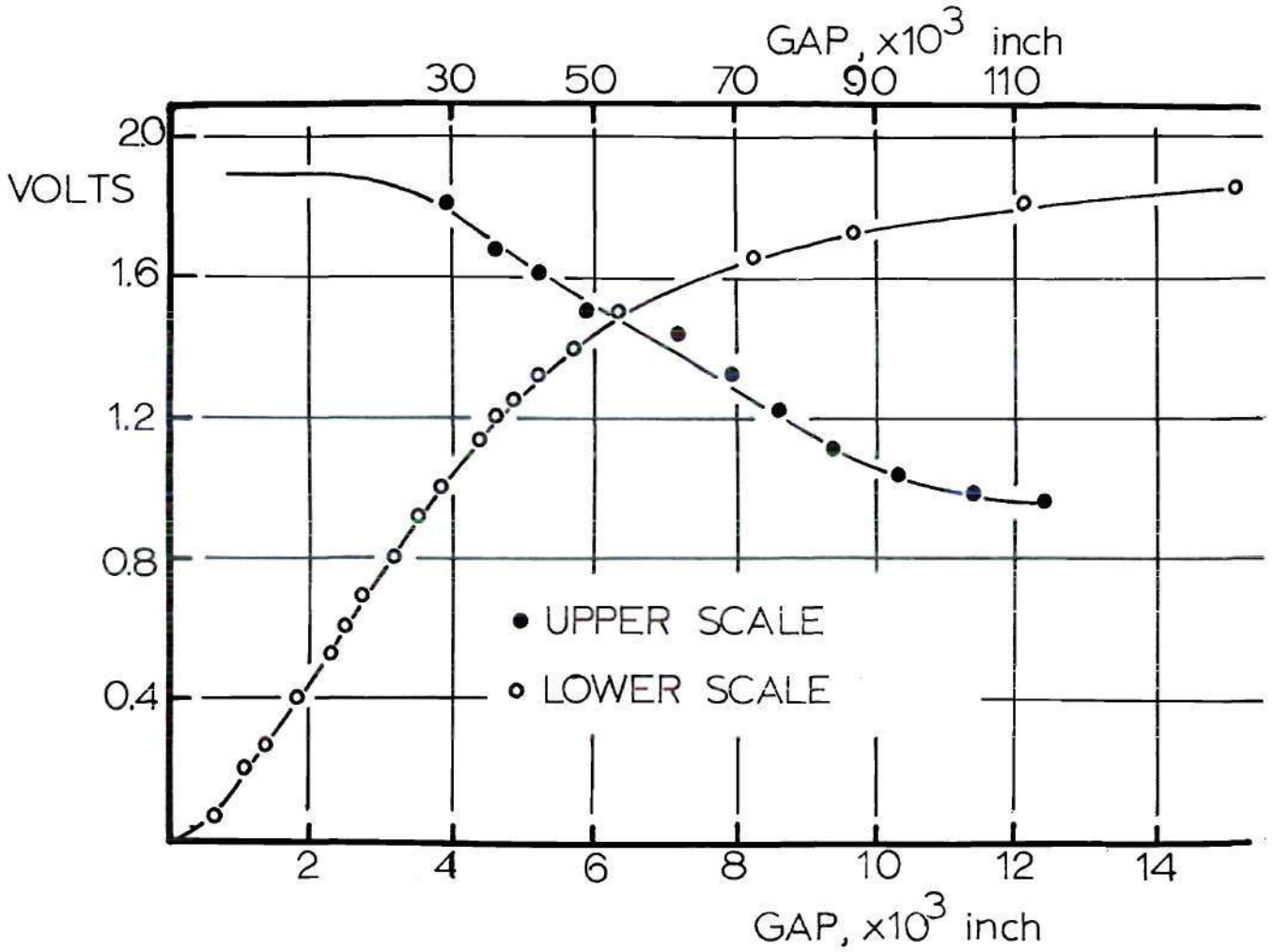


Figure 3. Voltage Calibration Curve for Fotonic Sensor

range for measurement of greater distances. As a first design consideration, therefore, a gap width or proximity range must be selected which gives a completely linear response on the higher sensitivity linear region.

Another important aspect of preliminary design is the selection of a proper material for the vibrating diaphragm or the transducing element. A list of guidelines to be followed for the proper selection of the diaphragm size and material is as follows:

1) Dimensions and total load must be compatible with physical properties of the material used.

2) Flexibility must be such as to provide the sensitivity required by the secondary transducer.

3) Volume of displacement should be minimized to yield an acceptable dynamic response.

4) Natural frequency of the membrane should be sufficiently high to provide satisfactory frequency response.

5) Force-deflection relationships must be linear.

6) Surface finish must be compatible with intensity levels for the photosensor.

On the basis of the criteria mentioned above, it may be concluded that the proper material should possess the reflectivity of a polished metal surface as well as the deformability of a material with a relatively low modulus of elasticity. A commercially available plastic material with an anodized aluminum deposit was selected as the diaphragm membrane. This material, distributed by the Dow Chemical Company, is commonly known by

its trade name of "Metallized Mylar." The elasticity modulus, E, of a Mylar material is approximately five hundred thousand pounds per square inch. The thickness selected was 0.00075 inch.

## Static Analysis of the Transducer

A circular diaphragm fixed at the circumference is a suitable geometry both from the viewpoints of convenience as well as the linear force-deflection relationship. With reference to the notation shown in Figure 4, the deflection of the membrane at any point, following Roark,[1] is given by

$$y = \frac{3W\,(m^2-1)\,(r_o^2 - r^2)^2}{16\pi\, E\, m^2 t^3\, r_o^2}\ , \tag{1}$$

where $y$ = deflection of the membrane, inches

$m$ = inverse of Poisson's ratio, $1/\nu$,

$r_o$ = diaphragm radius, inches

$t$ = thickness of the membrane, inches

$r$ = radial distance from the center of the undeflected membrane, inches

$W$ = total load applied, which is equal to $\pi\, r_o^2 \Delta P$, $lb_f$.

The radial stress, $\sigma_r$, is given by

$$\sigma_r = \frac{3W}{4\pi t^2}\ . \tag{2}$$

The deflection at the center is obtained from equation (1) by substitution of r=0. This gives the maximum deflection as

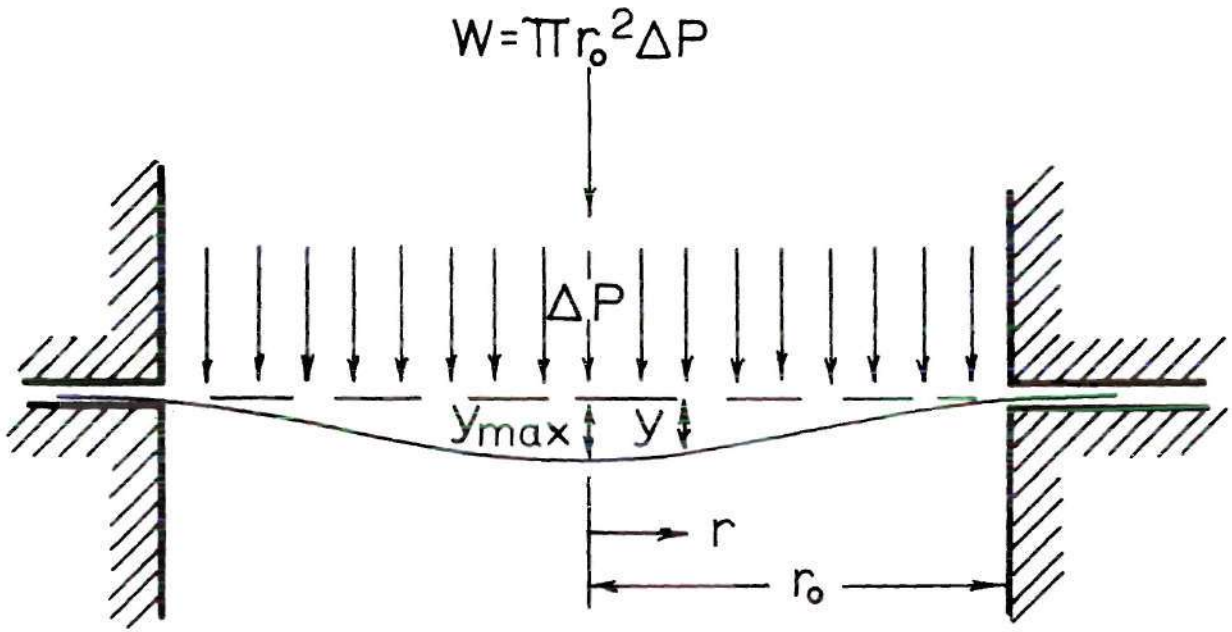


Figure 4. Nomenclature for Membrane

$$y_{max} = \frac{3\ (m^2-1)\ r_o^4}{16\ E\ m^2 t^3}\ \Delta P\ , \tag{3}$$

where W has been replaced by $\pi r_o^2 \Delta P$.

It may be noted that the expressions for the volume displaced and the membrane deflection are both dependent upon the membrane radius.

It was decided that a compact configuration of the transducer assembly with acceptable static and dynamic response would require a diaphragm of at least one eights of an inch radius. The volume displaced can be computed by integration of the deflection over the radius of a body of revolution varying from r=0 to r=$r_o$. This gives

$$Vol = \int_o^{r_o} 2\pi y r dr = \int_o^{r_o} \frac{3\ (m^2-1)\ \pi\Delta P\ (r_o^2-r^2)^2}{8\ E\ m^2 t^3}\ r dr = K\ \Delta P\ , \tag{4}$$

where W has been replaced by $\pi r_o^2 \Delta P$ and

$$K = \frac{(m^2-1)\ \pi\ r_o^6}{16E\ m^2 t^3}\ . \tag{4a}$$

The natural frequency of vibration of the membrane, following Miles,[2] is given by

$$f_r = 0.467\ t \left[\frac{E}{\rho(1-\nu^2)}\right]^{\frac{1}{2}} \frac{1}{r_o^2}\ , \tag{5}$$

where $f_r$ is the resonant frequency of the membrane and $\rho$ is its density.

Since there were no published data available for the material

properties of the diaphgram, the necessary constants were experimentally determined. In these tests the material was assumed to be isotropic, or having elastic properties independent of orientation. The test material was one inch wide, 0.00075 thick, and three inches long. A tensile test determined the yield point, yield stress, and elasticity modulus, E. A rectangular grid of known separation was drawn on the material before the test. After the test the same grid was measured again. From these data an experimental Poisson's ratio was determined. The stress-strain graph for the material is shown in Figure 5. The results obtained from the experiments may be quoted as

$$E = 501{,}000, \text{ psi} \tag{6}$$

$$\sigma_{yield} = 9{,}550, \text{ psi}$$

$$\nu = 0.45$$

Substitution of these values into equation (2) yields the maximum pressure that can be applied to the membrane as

$$\Delta P = \left(\frac{0.45}{\text{Safety factor}}\right), \text{ psi} \tag{7}$$

The maximum deflection calculated from equation (3) is given by

$$y_{max} = \left(\frac{0.0771}{\text{Safety factor}}\right), \text{ inches} . \tag{8}$$

The constant K of equation (4) has a value of

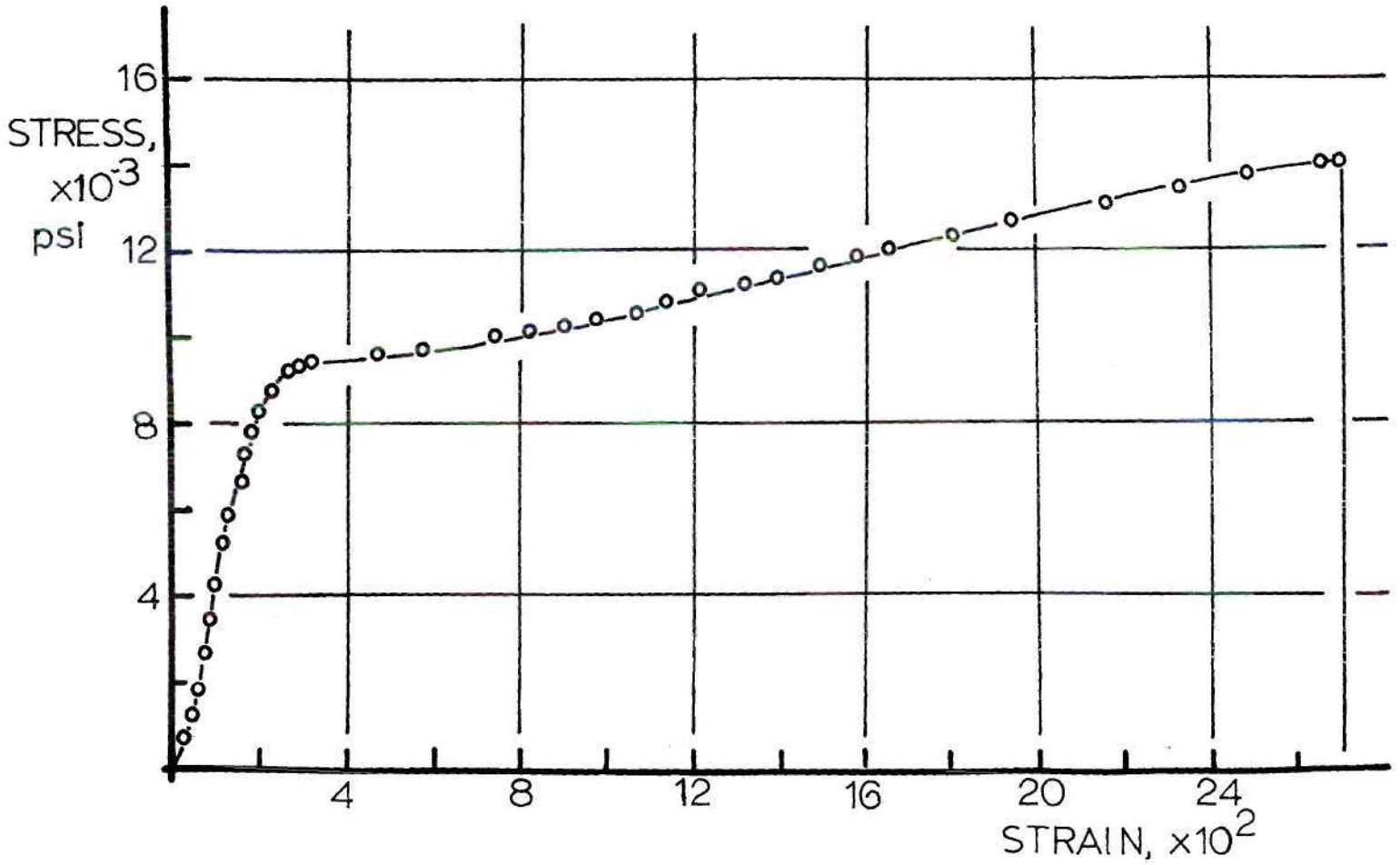


Figure 5. Experimental Stress-Strain Curve for Mylar

$$K = 2.79811 \times 10^{-3}, \text{ in}^5/\text{psi} . \quad (9)$$

The density[3] of the material is 2.4902, slugs/ft$^3$, which is substituted with the physical constants in equation (5). This results in

$$f_r = 1{,}588.67, \text{ cycles/second} \quad (10)$$

as the resonant frequency for the membrane.

## Dynamic Analysis of the Transducer

Two basic types of dynamic flow and pressure fields involve either the establishment of a steady flow following a disturbance or continual periodic oscillations. Analysis of the transient behavior of a pressure transducer is complicated due to the introduction of time as an additional variable, and also due to the problem of phase shift in a dynamic pressure pulse as it propagates through connecting lines and passages.

Most flow systems have fluctuations that may affect pressure measurements. In order for the measuring transducer to record the correct pressure, the dynamic characteristics of the measuring system must be isolated and identified. It is recognized immediately that a rigorous dynamic analysis of the pressure transducer system is an extremely difficult task; this, however, does not preclude an attempt to analyze a simplified model of the entire system.

Toward this end of a simple dynamic analysis, consider the transducer system to be represented by a cavity at the termination of a connecting line, as shown in Figure 6. The volume of gas in such a pressure

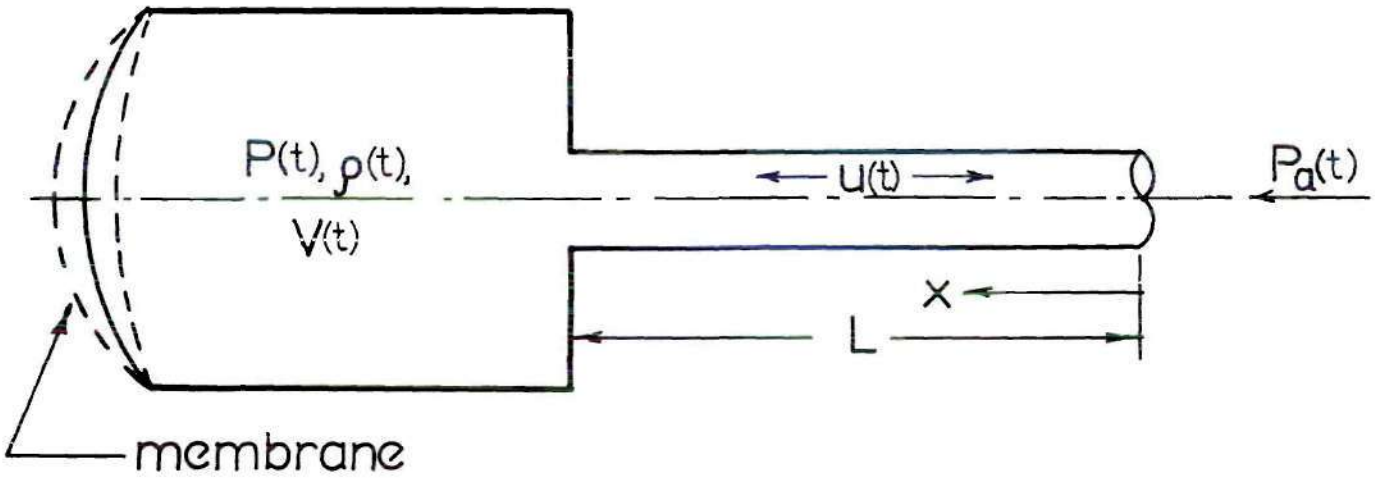


Figure 6. Sketch of Transducer

transducer system may be considered as a simple vibration system. The purpose of the analysis is to predict the fluctuating signal, $p_a(t)$, at the entrance of the connecting line. It is reasonable, from a practical application viewpoint, to limit the analysis to a signal which consists of a fluctuating signal of relatively small amplitude superimposed on a time averaged mean signal of relatively large amplitude.

A great deal of simplification in the analysis can be accomplished by considering two limiting cases for the compression process in the transducer system. The first case considers the connecting line volume to be negligible in comparison to the volume of the transducer cavity. The other case neglects the cavity volume in comparison to the connecting line volume. The actual results should lie somewhere in between these two cases. The basis of this approach is the fact that it is easier to calculate the pressure response of the transducer in terms of two simplified limiting cases than it is to calculate the combined effect of the limiting cases simultaneously.

In the first case the volume of the connecting line is less than that of the cavity. It means that most of the compression may be considered to be taking place in the cavity, thus allowing the simplified assumption that the gas motion in the tube is incompressible. The gas mass in the tube then acts like an oscillating mass in a gas spring made up of the compressible gas in the cavity.

Since the gas column in the tube is considered to be incompressible, the pressures at the entrance and at the exit of the connecting line are in phase. In other words, transmission of signal through the

tube is instantaneous. Denoting the pressure in the cavity as p(t) and the pressure, $p_a(t)$, as the input pressure to the line, the problem must be considered with respect to force and acceleration of the gas in the tube. Pressure oscillations are assumed to be of sufficiently small amplitude (with respect to the value of mean pressure) so as to render the volume flow in and out of the tube much less than the volume already contained in the tube. As a result, friction may be neglected for a first order analysis; but the effect of friction as resistance in the tube must be taken into account. The time dependent variables are: i) the pressures, p(t) and $p_a(t)$; ii) density, $\rho$, in the cavity; and iii) gas velocity or displacement in the tube.

Under the assumptions made in the preceding discussion, the dynamic equation for the gas in the tube is

$$p(t)A - p_a(t)A = \rho AL \frac{du}{dt} + FCLu \ , \tag{11}$$

where u is the streamwise velocity in the line, A is the area of cross section of the tube, L is the length of the tube, C is the perimeter of the tube, and F is the tube shear-resistance constant. Assuming laminar flow rate, the constant F is given by

$$F = \frac{8\mu}{d} \ , \tag{12}$$

where $\mu$ is the fluid viscosity and d is the tube diameter.

The continuity equation may be written as

$$\frac{d}{dt}\left(M_{cavity}\right) + \rho A u = 0 \ , \tag{13}$$

where $M_{cavity}$ is the mass of fluid in the cavity. The temporal variation of mass is given by

$$\frac{dM_{cavity}}{dt} = \rho \frac{dV}{dt} + V \frac{d\rho}{dt} \ , \tag{14}$$

where V is the volume of the cavity. The first term on the left side of equation (14) is the change of mass due to the displacement of the membrane and the second term is that due to the compression of the fluid. The change of mass due to the membrane can be obtained from equation (4) as

$$\frac{dV}{dt} = K \frac{dp}{dt} \ , \tag{15}$$

where K is the volume displaced by the membrane per pound per square inch applied, as was discussed in the static analysis.

For a low viscosity fluid, friction and heat transfer may be neglected so that the pressure density variation process may be considered isentropic which is described by

$$\frac{dp}{d\rho} = \frac{a^2}{g_c} \tag{16}$$

or

$$\frac{d\rho}{dt} = \frac{g_c}{a^2} \frac{dp}{dt}$$

where a is the acoustic speed in the medium. The variation of pressure and density are small enough, so that the acoustic speed is considered constant. When equations (13-16) are combined one obtains

$$u = - \left( \frac{Vg_c}{A\rho a^2} + \frac{K}{A} \right) \frac{dp}{dt} . \tag{17}$$

When equation (17) is differentiated with respect to time, and when second order variations involving the product of two differentiation quantities are neglected, the result incorporated into equation (11) gives

$$\rho L \left( \frac{Vg_c + K\rho a^2}{\rho A a^2} \right) \frac{d^2 p}{dt^2} + \frac{FLC}{A} \left( \frac{Vg_c + K\rho a^2}{\rho A a^2} \right) \frac{dp}{dt} + p = p_a . \tag{18}$$

The initial conditions on the system are

$$\left.\begin{aligned} p &= P_o \\ \frac{dp}{dt} &= J \end{aligned}\right\} \quad \text{at } t=0 , \tag{19}$$

where $P_o$ is a mean pressure and J is a constant. Equation (18) can be solved in the Laplace transform domain as

$$\frac{P_{(s)}}{P_a(s)} = \frac{1 + \frac{p_o}{P_a} \left( \frac{s}{\omega_n^2} + \frac{2\xi}{\omega_n} \right) + \frac{J}{\omega_n^2 P_a}}{\frac{s^2}{\omega_n^2} + \frac{2\xi s}{\omega_n} + 1} , \tag{20}$$

where

$$\omega_n = \left[ \frac{1}{\rho L} \left( \frac{\rho A a^2}{Vg_c + K\rho a^2} \right) \right]^{\frac{1}{2}} , \tag{21}$$

and

$$\xi = [\rho L]^{\frac{1}{2}} \left[\frac{Vg_c + K\rho a^2}{\rho A a^2}\right]^{\frac{3}{2}} \frac{FLC}{2} \quad . \tag{22}$$

Equation (20) describes the system response to a sinusoidal input. Therefore, if the input $p_a(t)$ is composed of a mean pressure, $P_o$, and a superimposed sinusoidal pressure, the Laplace transform of $p_a(t)$ is

$$P_a(s) = \frac{P_o}{s} + \frac{P_w \omega}{s^2 + \omega^2} = \frac{P_o (s^2+\omega^2) + P_w \omega s}{s(s^2 + \omega^2)} \quad , \tag{23}$$

where $P_w$ is the amplitude of the oscillating signal and $\omega$ is its frequency. When all transients die out, the output is a sine wave of the same frequency as the input. However, the amplitude of the output may differ from that of the input and a phase shift may be present. Since the frequency is the same, the relation between the input and output sine waves is completely specified by giving their amplitude ratio and phase shift. Since, in general the frequency response of a system consists of the curves of amplitude ratios and phase shifts as functions of frequency, the steady-state amplitude ratio and phase shift can be determined by replacing s with $j\omega$ in the system's transfer function.[4] When s is replaced by $j\omega$ in equation (23), it results in an infinite value for $P_a$. Incorporation of this result into equation (20) and replacement of s by $j\omega$ gives

$$\frac{P(j\omega)}{P_a(j\omega)} = \frac{1}{\left(\frac{j\omega}{\omega_n}\right)^2 + \frac{2\xi}{\omega_n}(j\omega) + 1} \quad . \tag{24}$$

This is a second-order transfer function where $\omega_n$ is the resonant frequency of the system and $\xi$ is the damping ratio. The magnitude or gain is given by

$$\left|\frac{P(j\omega)}{P_a(j\omega)}\right| = \frac{1}{\left\{\left[1 - \left(\frac{\omega}{\omega_n}\right)^2\right]^2 + \left(\frac{2\xi\omega}{\omega_n}\right)^2\right\}^{\frac{1}{2}}} , \tag{25}$$

and the phase shift, $\phi$, is given by

$$\phi = \tan^{-1} \frac{-2\xi\omega/\omega_n}{1 - \left(\frac{\omega}{\omega_n}\right)^2} . \tag{26}$$

A theoretical frequency response obtained by substituting the values for the constants and different frequencies in equations (25) and (26) is shown in Figure 7.

It was pointed out earlier that the other limiting case of dynamic analysis is obtained when the volume of the transducer cavity is considered to be significantly less than the volume of the connecting line. In this case most of the compression takes place in the line, which allows the simplified assumption that the gas motion in the transducer cavity is incompressible, and that the signal is propagated instantaneously.

The two basic equations governing transient flow in pipes in terms of the notation explained earlier, are written, following Schuder,[5] as

$$\frac{\partial u}{\partial x} = - \frac{1}{\rho a^2} \frac{\partial p}{\partial t} , \tag{27}$$

and

$$\frac{\partial p}{\partial x} = -\rho \frac{\partial u}{\partial t} - Ru , \tag{28}$$

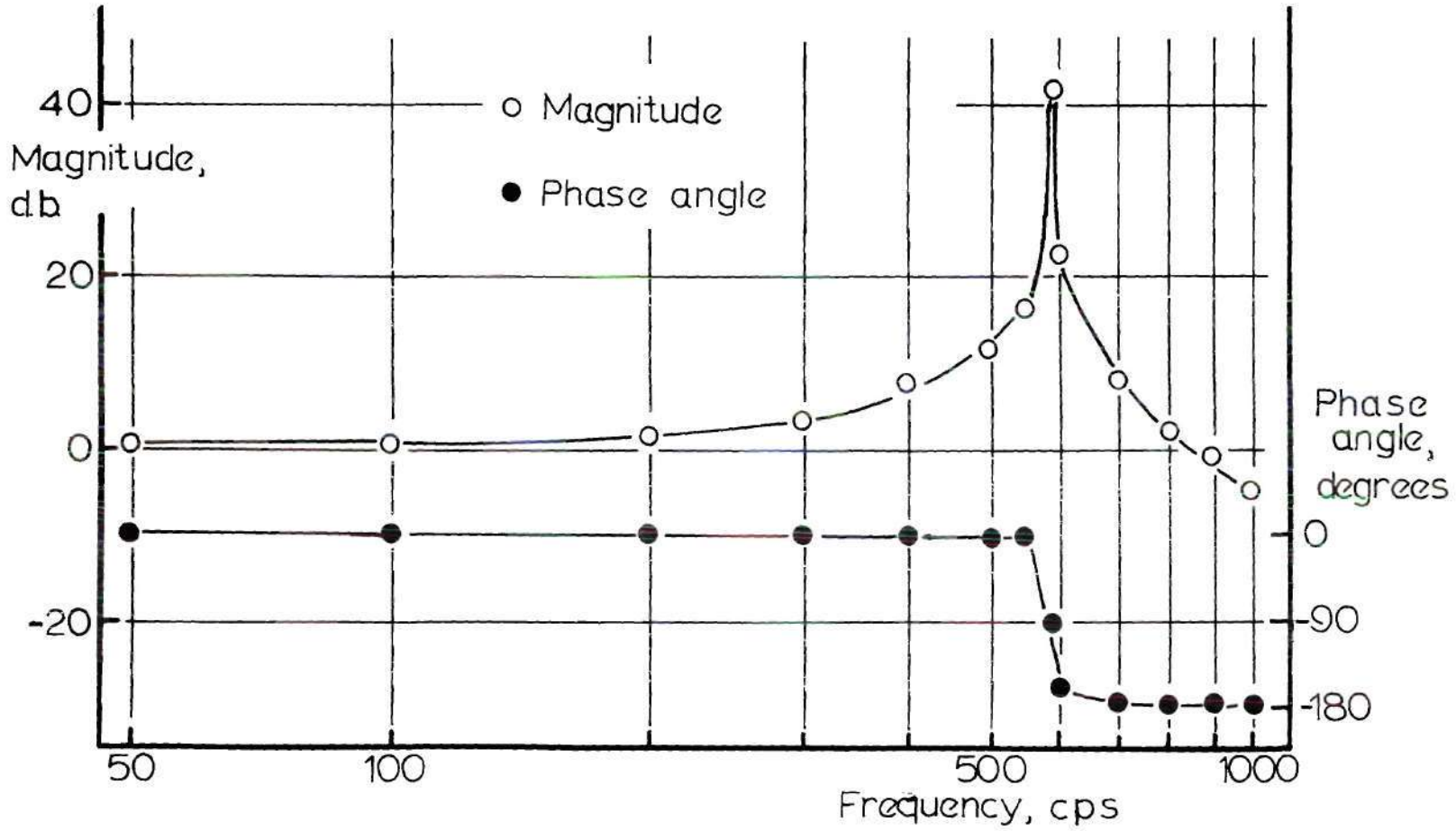


Figure 7. Frequency Response to Small Line Volume Transducer Model

where x is the distance along the line and R is the frictional resistance. These equations are based on the assumption of an adiabatic flow of a compressible fluid with friction, but without rigorously taking into account the velocity gradient across the tube. The flow is assumed laminar which is justified due to the small flow rate that is expected.

The Laplace transform of equations (25) and (26), respectively, is

$$\frac{\partial V}{\partial x} = - \frac{1}{\rho a^2} (sP - p(x,0)) , \tag{29}$$

and

$$\frac{\partial P}{\partial x} = - \rho (sV - u(x,0)) - RV , \tag{30}$$

where $p(x,0)$ and $u(x,0)$ are the initial conditions at any location x. The initial conditions may be expressed as

$$p(x,0) = P_o \quad \text{and} \quad u(x,0) = 0 . \tag{31}$$

Differentiation of equation (30) with respect to x and substitution of equation (29) into the result gives

$$\frac{\partial^2 P}{\partial x^2} - (R + \rho s) \frac{s}{\rho a^2} P = - (R + \rho s) \frac{1}{\rho a^2} P_o . \tag{32}$$

The general solution of this equation is of the form

$$P(x,s) = G e^{\beta x} + H e^{-\beta x} + \frac{P_o}{s} , \tag{33}$$

where G and H are arbitrary functions and $\beta = [(R + \rho s)\ s/\rho a^2]^{\frac{1}{2}}$.

The constants G and H may be determined from the two boundary conditions. The first of these boundary conditions is

$$\text{at}\quad x=0 :\quad p(o,t) = P_o + P_w \sin\omega t\ , \tag{34}$$

with its Laplace transform

$$P(o,s) = \frac{P_o}{s} + \frac{P_w\ \omega}{s^2 + \omega^2} = \frac{P_o\ (s^2 + \omega^2) + P_w\ \omega s}{s(s^2 + \omega^2)}\ . \tag{35}$$

The second boundary condition obtained by considering that at x=L, the mass flow rate into the terminal volume equals the rate of mass increase within the volume. In order words,

$$\rho A\ u(L,t) = V\ \frac{d\rho}{dt} + K\rho\ \frac{dp}{dt}\ . \tag{36}$$

With the assumption that the change in terminal volume occurs adiabatically and reversibly, i.e.,

$$\frac{dp}{d\rho} = \frac{a^2}{g_c} \tag{37}$$

one obtains

$$u(L,t) = \left(\frac{Vg_c}{\rho A a^2} + \frac{K}{A}\right) \frac{dp}{dt}\ . \tag{38}$$

The Laplace transform of equation (38) is given by

$$V(x,s) = \left(\frac{V + K\rho a^2}{A\rho a^2}\right) [sP(x,s) - p(L,0)] , \tag{39}$$

where $p(L,0)$ is the pressure at the end of the line and is equal to $P_o$. Therefore, at x=L, one obtains

$$V(L,s) = \left(\frac{V + K\rho a^2}{A\rho a^2}\right) [sP(L,s) - P_o] . \tag{40}$$

One next differentiates equation (33) with respect to x and evaluates the derivative at x=L. The resultant expression and equation (40) are incorporated into equation (30) to give

$$G\left[1 - \beta\left(\frac{V + K\rho a^2}{A}\right)\right] e^{-\beta L} = H\left[1 + \beta\left(\frac{V + K\rho a^2}{A}\right)\right] e^{-\beta L} , \tag{41}$$

where $P(L,s)$ has been evaluated from equation (33) at x=L, and has been substituted into equation (40). Equation (33) is evaluated at x=0 and is combined with equation (35) to give

$$G + H = \frac{\omega P_w}{s^2 + \omega^2} . \tag{42}$$

Equations (41) and (42) are combined to give G and H as

$$G = \frac{P_w \omega T e^{-2\beta L}}{(s^2 + \omega^2)(1 + T e^{-2\beta L})} , \tag{43}$$

and

$$H = \frac{P_w \omega \, T \, e^{-2\beta L}}{(s^2 + \omega^2)\,(1 + Te^{-2\beta L})} ,$$

where

$$T = \frac{1 - \beta\left(\frac{V + K\rho a^2}{A}\right)}{1 + \beta\left(\frac{V + K\rho a^2}{A}\right)} .$$

With the functions as determined in the preceding analysis, the solution of equation (33) is obtained as

$$P(x,s) = \frac{P_w \omega}{(s^2 + \omega^2)\,(1 + Te^{-2\beta L})}\left[Te^{-\beta(x-2L)} + e^{-\beta x}\right] + \frac{P_o}{s} . \qquad (44)$$

The gain of the system is

$$\frac{P_{out}}{P_{in}} = \frac{P(L,s)}{P(o,s)} = \frac{s\,\omega\,P_W\,(T\,e^{-\beta L} + e^{-\beta L}) + P_o\,(s^2 + \omega^2)\,(1 + Te^{-2\beta L})}{(1 + T\,e^{-2\beta L})\,(P_o\,s^2 + P_o\,\omega^2 + s\,\omega\,P_w)} . \qquad (45)$$

Replacement of s by jω in equation (45) gives

$$\frac{P_{out}}{P_{in}} = \frac{[1 + T(j\omega)]\,e^{-\beta(j\omega)L}}{1 + T(j\omega)\,e^{-2\beta(j\omega)L}} . \qquad (46)$$

Magnitude and phase angle of this transfer function may be obtained with the substitution of numerical values for the frequency ω. It may be noted that T and β depend on jω, and, therefore, they have both magnitudes and phase angles. However, for very short lines the exponential term in equation (46) is approximately unity because the exponent is very small. This

leads to the conclusion that there are no losses and no phase shifts in the line as is to be expected. If the length of the line increases, a phase shift is obtained from equation (46).

For a typical application of the transducer the connecting line would be expected to be of rather short length. For such a case, the analysis which neglects cavity volume would yield no phase shift in the pressure pulse during propagation. Since this deduction is not very realistic, it is expected that the experimental results would be closer to the results of the analysis of the first case which neglected the line volume in comparison to the cavity volume.

# CHAPTER III

## EXPERIMENTAL PROGRAM

### Mechanical Design of Transducer Assembly

In order to check the analytical predictions of transducer performance, an experimental program was initiated. A transducer assembly was designed, fabricated, and tested for static and dynamic performance with suitable test instrumentation. The mechanical design of the transducer system was based on the requirements that

i) a quarter of an inch diameter membrane must be clamped along its circumference to simulate a dynamic performance of an elastic plate. The membrane diameter was selected for a compact transducer configuration and uniform pressure distribution,

ii) the design must allow for a convenient way to replace the diaphragm,

iii) the pressure side of the transducer must be satisfactorily sealed, and

iv) the design must incorporate a scheme for holding the fotonic sensor probe steady, centered and normal to the undeflected membrane.

Although the transducer design was expected to be applicable for both gage and differential pressure measurements, it was considered sufficient to use standard atmospheric pressure on one side of the diaphragm for the purpose of demonstrating the feasibility of this instrument. The other side of the membrane was subjected to a very low pressure signal

that was to be measured. It may be worth noting that the analysis developed in Chapter II for a differential pressure signal is equally applicable to the experimental model using standard atmospheric pressure as a reference.

In the cross sectional view of the pressure transducer shown in Figure 8, the sensor membrane is placed in between the low pressure chamber and the fotonic proximity sensor. Before assembly the membrane was slightly pre-stressed to preclude its wrinkling and initially assure a flat surface. A holding ring with an inner diameter slightly greater than the outer diameter of the container was used to hold the membrane in between the two rings. This assured a firm and stretched-flat membrane surface with zero differential pressure across it. Since metal-to-metal contact was not deemed enough to prevent leakage, two urethane seals were used for the low pressure chamber. This also resulted in providing an initial circumferential stress on the membrane, thus assuring a clamped plate type of behavior.

An eighth of an inch diameter hole was provided to guide the fotonic proximity sensor, the latter having an outer diameter of about 0.109 inch. Such an arrangement assured the probe of remaining normal to the membrane surface. The long guide hole was terminated by a short length of a larger diameter hole of one quarter of an inch. This region was in the immediate vicinity of the membrane. The inside surface of the hole was painted black so as to avoid stray reflections. Finally, a large nut was used to hold the components together.

It was pointed out earlier that the fotonic sensor output varied

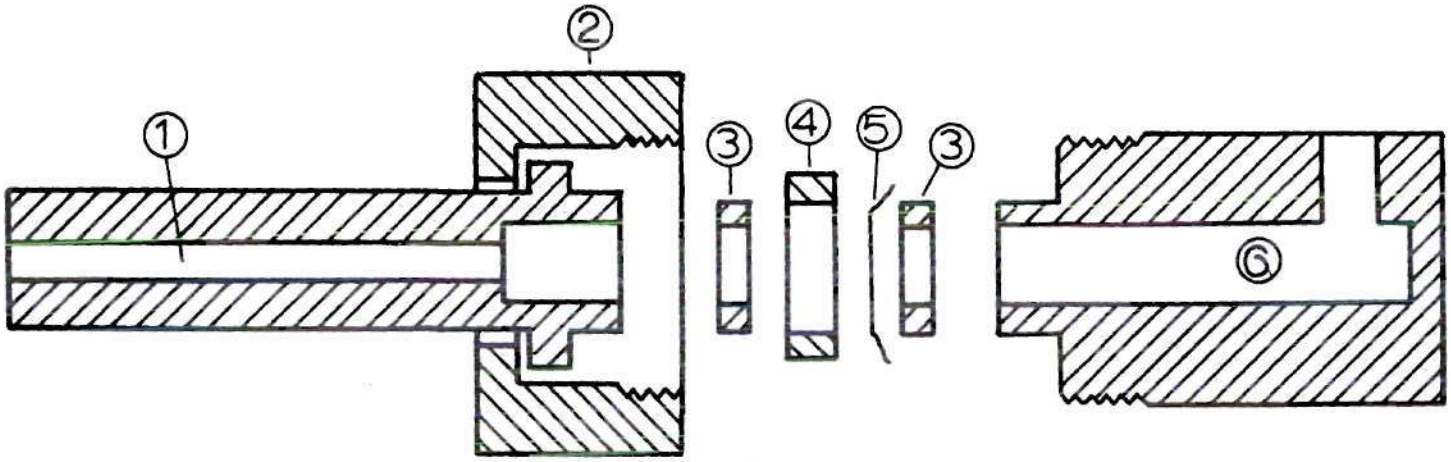


① Guide hole for fotonic proximity sensor

② Nut

③ Sealing rings

④ Holding ring

⑤ Membrane

⑥ Container

Figure 8. Sectional View of Pressure Transducer

inversely with its proximity from the flat surface, and also that it had a rather limited range of high sensitivity. The equilibrium or null position of the sensor was selected a few thousandths of an inch from the membrane to yield the most favorable calibration. In order to measure very small variations of the proximity from this null position a separate mechanism was incorporated into the design. The fotonic sensor was mounted at one end of an arm which was held steady by a retaining screw as shown in the sketch in Figure 9. The other end of the arm was attached to a micrometer with an arm length lever ratio of one to four. This increased the sensitivity of null position adjustment of the sensor by a factor of four. For coarse horizontal adjustments and for change in the height of the arm from a base, further provisions were also made. To assure a positive control the arm was spring loaded.

Finally, the transducer assembly and fotonic sensor adjustment mechanism were mounted on a firm base with rubber pads to isolate the system from stray vibrations. A photograph of the test assembly is shown in Figure 10.

## Test Arrangements and Instrumentation

For experimental evaluation of the transducer performance, two different schemes were used to generate suitable reference pressure signals. Figures 11(a) and 11(b) show, respectively, a block diagram and a photograph of the static test arrangement. Figures 12(a) and 12(b) show, respectively, a block diagram and a photograph of the dynamic test arrangements. To affect a small change in the static pressure input to the transducer a piston-cylinder arrangement was designed. This arrangement is

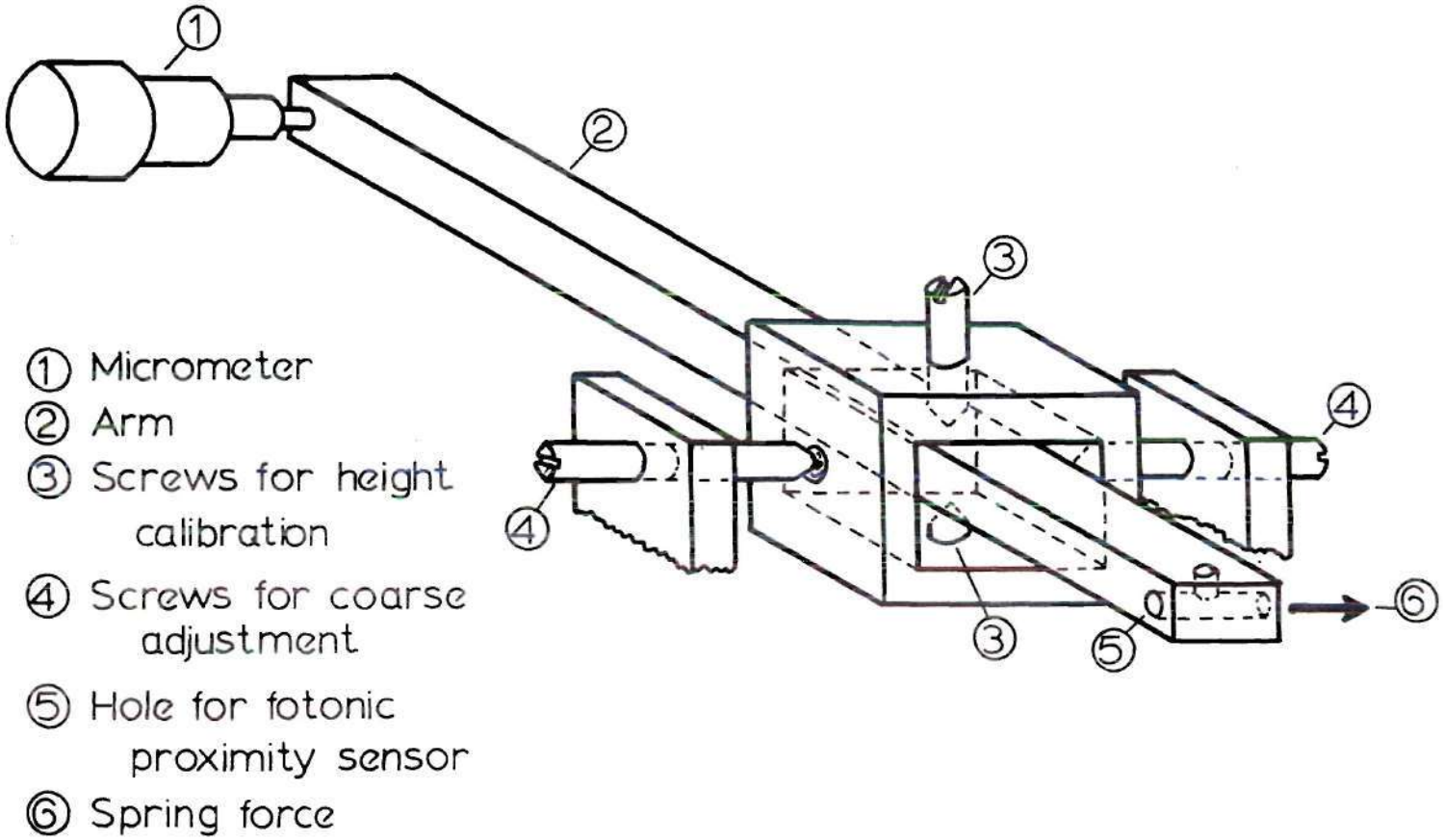


Figure 9. Sketch of Fotonic Sensor Probe Arm Mechanism

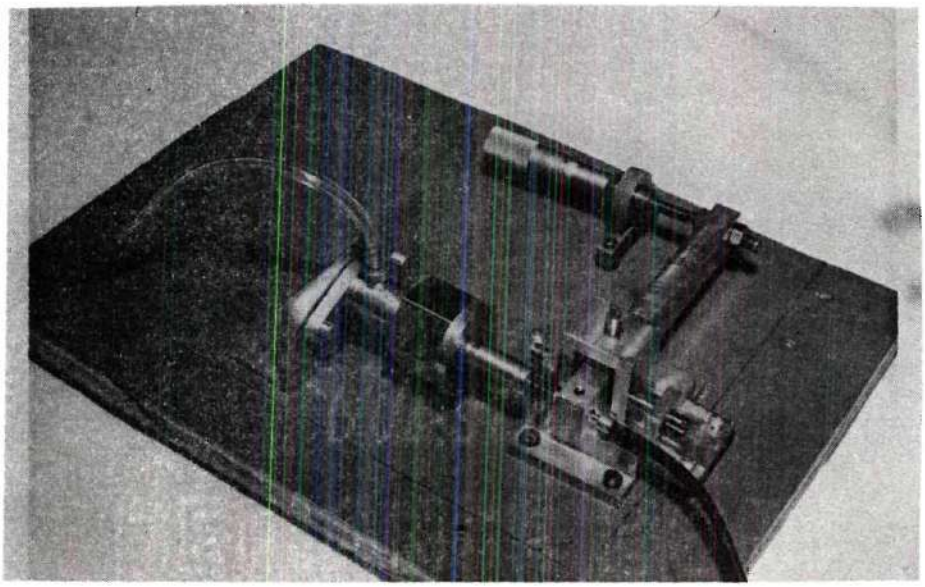

Figure 10. Pressure Transducer Test Assembly

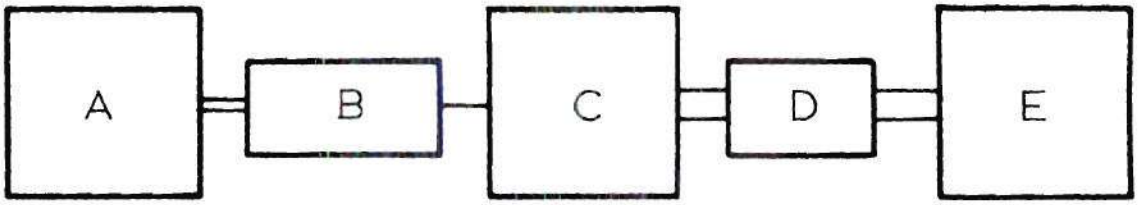


A Static Pressure Signal Generator
B Transducer
C Fotonic Sensor
D Filter
E Display

(a) schematic

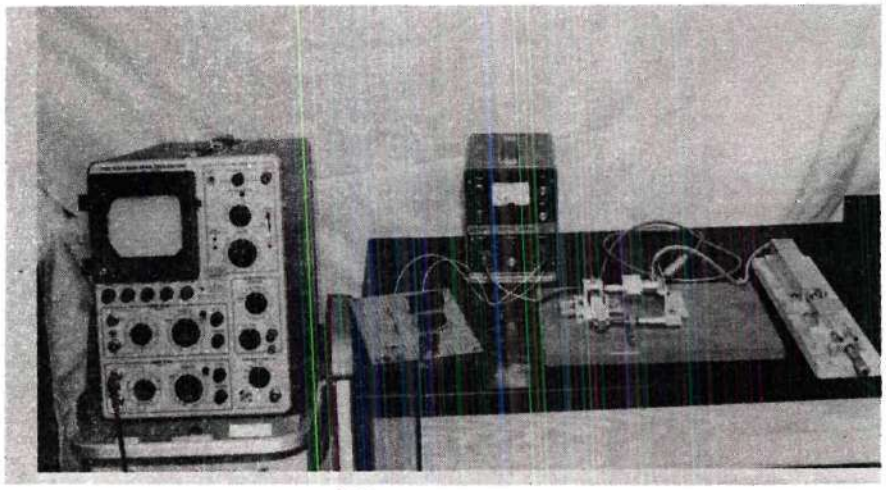

(b) actual test set-up

**Figure 11. Static Test Arrangement**

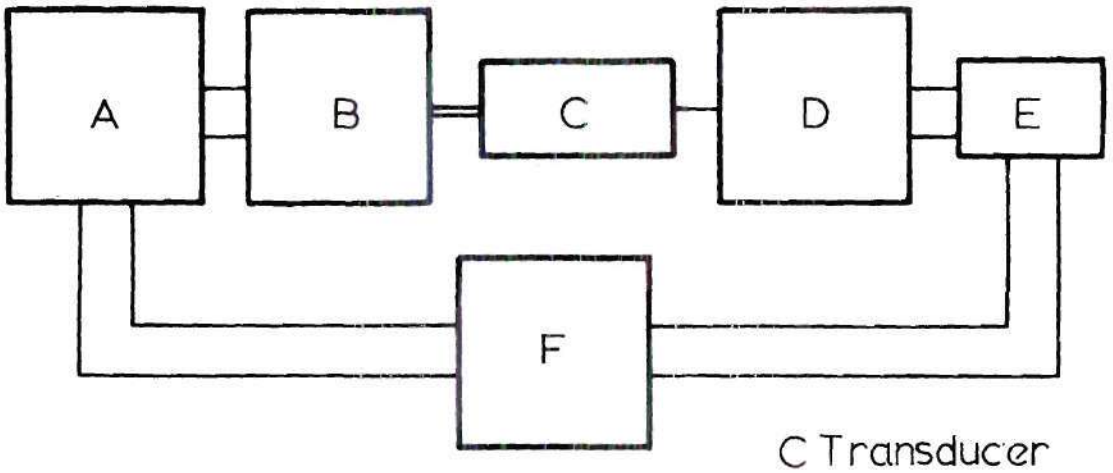


A Electrical Signal Generator
B Dynamic Pressure Signal Generator
C Transducer
D Fotonic Sensor
E Filter
F Phase and Magnitude Measuring device

(a) test set-up schematics

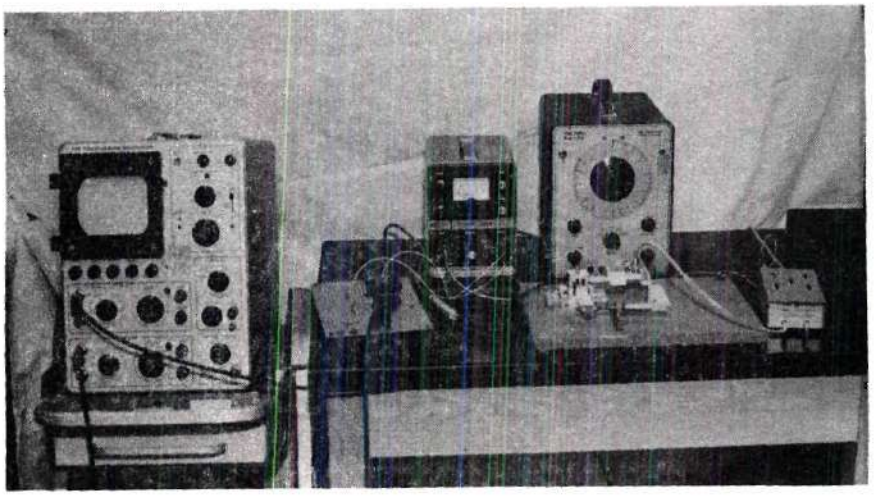

(b) test set-up

**Figure 12. Dynamic Test Arrangement**

shown in Figure 11(b). For initial chamber volume and mean pressure of $V_c$ and $\bar{p}_c$, respectively, the change in the pressure corresponding to the advance of the piston in the cylinder can be computed for an assumed isothermal process from

$$d\bar{p}_c = \beta \frac{dV_c}{V_c} , \tag{47}$$

where $\beta$ is the bulk modulus of air in the cylinder. It may be pointed out that the chamber volume considered here must include that of the connecting line to the transducer. For the one inch diameter piston used in these tests, the change in volume in cubic inches, for a piston displacement of $\ell$ inches, is given by

$$\Delta V_c = (0.785)\ \ell,\ \text{in}^3 . \tag{48}$$

When the connecting line and fitting volumes are added to the volume of the chamber, the total volume is 6.30 cubic inches. The displacement of the piston was measured by a micrometer. A static calibration curve relating pressure to the transducer output voltage may be represented as a calibration curve relating the latter with the piston displacement by a proper scale change. It is worth noting here that, to obtain reproducible data, it was considerably more convenient to use the output voltage change rather than the voltage level itself. This was due to the difficult task of obtaining an adjustable null voltage for a selected size of the gap between the membrane and the fotonic sensor. The null position was so adjusted that the fotonic sensor output voltage variation, resulting from

the gap variation, occurred in the linear range of the sensor output characteristics. Finally, a combination of equation (3) relating change in pressure to the maximum deflection of the membrane, equation (47) relating change in pressure to the change in volume, equation (48) relating change in volume to the piston displacement, and the voltage output characteristic curve of the sensor, shown in Figure 3, resulted in the relation

$$\Delta E = (0.274)\ y_{max}\ ,\ \text{volts}, \tag{49}$$

where $\Delta E$ represents the change in the output voltage which was recorded. In equation (49) $y_{max}$ is measured in thousandths of an inch.

Results of static tests were compared with the analytically predicted values.

The dynamic studies used a sinusoidal reference pressure signal generator with adjustable frequency and amplitude, manufactured by General Electric Company. Figure 13 shows the schematic of this device consisting of an air supply line, a fixed resistance, a flapper-nozzle arrangement, and a torque motor. Varying frequency sinusoidal pneumatic wave forms could be readily produced by driving the torque motor with an electronic function generator. The oscillations of the motor cause the flapper motion which vary the back pressure resistance of the nozzle. In essence this arrangement corresponds to a Wheatstone bridge with two fixed resistances and two variable ones. The resulting output pressure level and its frequency were adjusted by selecting a suitable air supply pressure and electronic signal generator frequency.

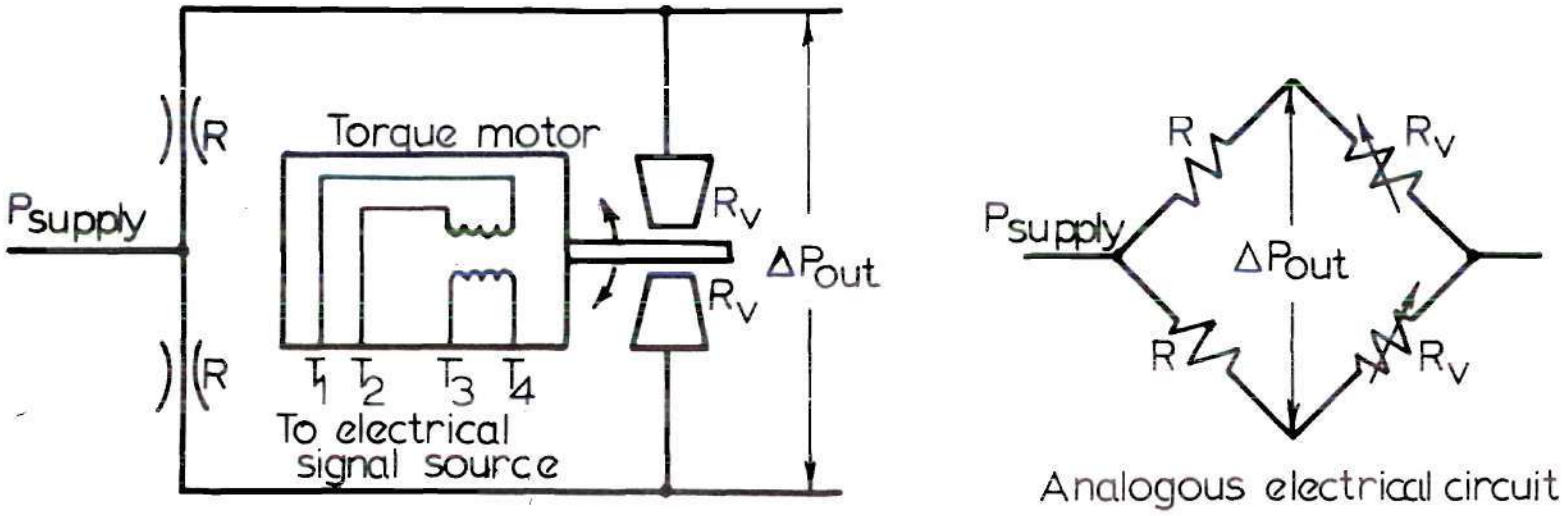


Figure 13. Pressure Signal Generator Schematic and Electrical Analog

A Pitran pressure transducer, PT-2, commonly used in fluidic circuit tests, was utilized to study the pressure response of individual components of the block diagram shown in Figure 11(a), as well as to obtain the overall frequency response of the system. The pressure transducer, PT-2, has a sensitivity of 1.647 Volts/psig. It also has a flat frequency response up to one megacycle.

A two-channel oscilloscope was utilized to display the frequency responses, which were photographed. Both ac and dc measurements were made from the displays. A combination digital voltmeter/printer was also used as an alternate way of obtaining data. However, undesirable signal to noise characteristics of the digital device resulted in its limited utilization. A photograph of the dynamic test arrangement is shown in Figure 11(b). Finally, it may be pointed out that all the tests were performed under constant temperature conditions.

## Description of the Tests

Prior to conducting either static or dynamic performance tests, a calibration was made of the fotonic sensor output voltage for variable gap distances between the transducer membrane and the fotonic sensor. In order to operate within the linear range of sensor output it was necessary to select initial gap distances. The sensor output was directly calibrated in terms of the gap widths. The procedure for the calibration is summarized as follows:

i) With minimum light intensity, set the fotonic sensor at zero gap width and adjust the sensor output current scale to zero.

ii) Determine the output range (upper limit) of the sensor by

increasing the light intensity gradually to cover one hundred percent of the current scale.

iii) Set the gap width so as to obtain forty percent of the maximum output on the current scale to operate within the linear range of the sensor.

It was observed that the instrument output voltage, rather than the current, could be measured with better resolution. As a result the output voltage of the sensor was fed into the oscilloscope.

The first series of tests attempted were for the static performance. It was observed that stray noise and dc drift were responsible for degrading the signal. It was suspected that the high sensitivity of the sensor, together with thermal heating from light source and a limited stability of the power supply resulted in a noisy signal with dc drift. Since the transducer was originally conceived to be suitable for measurement of pressures of the order of thousandths of a psi, it was deemed necessary to use the highest sensitivity range of the fotonic sensor. After several attempts at filtering the signal, combined with suitable vibration isolation and shielding of the system, only marginally acceptable signals were obtained in the static performance studies. The least objectionable filter had a time constant of two seconds. This filter and its transfer function are shown in Figure 14. It might be noted that the problem of drift was more severe than that of noise. This was found to be peculiar to the linear range of sensor operation. Further attempts to isolate the drift by observing the rate of change of the presumed dc output did not yield any better insight into the problem.

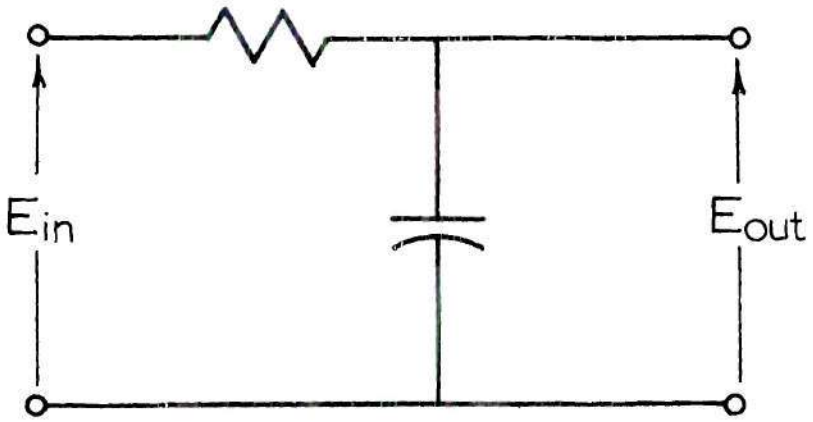


$$\frac{E_{out}}{E_{in}} = \frac{1}{RCs+1}$$

Figure 14. Filter Circuit and Transfer Function

Notwithstanding the fact that very low pressure levels were examined in these tests, the possibility of leakage through connectors, fittings, and piston clearance could not be totally discarded. However, incorporation of special vacuum fittings as well as more extensive sealing techniques did not result in any significant improvement in signal quality.

Attempts to obtain digital printouts of the signal for statistical analysis of the drifting signal were foiled by the fact that the digital read-out system added undesirable noise.

It is the opinion of the writer that the source of the drift problem was the fotonic sensor system itself. This system contained a regulated power supply to the light source and the photocell, the output of the latter being amplified with a transistor. Since the transistor works with current rather than voltage, it was not possible to detect the character of the transistor without isolating the component. It was observed that, although the regulated power supply voltage was stable within 0.2 percent, the photocell output was considerably more noisy. To make further conjecture, the source of drift may be attributed to i) a noisy transistor preceding the light source (photocell and light source operate at constant supply voltage), thus affecting the light intensity, ii) a faulty transistor following the photocell, iii) an undesirable photocell output, and iv) the open-loop circuit giving instability. It is worth noting that the curves shown in Figures 2 and 3 were obtained after replacing the original transistors with new ones.

It must be recognized that all photocells possess some drift ex-

pressed as a percentage of the nominal resistance. It is thought that the one with less than five percent drift should be acceptable for the present application. The cell in the fotonic sensor was tested for its performance. A light bulb fed by dc batteries was used as a source of constant intensity for the test. The bulb intensity at six volts dc supply corresponded to the maximum intensity of the sensor. Figure 15 shows this test arrangement, where the cell was mounted at one end of an enclosed tube, with the light source at the other end. Accurate measurements of the current from the photocell indicated less than one and one quarter of a percent drift for low intensity tests. At higher intensities the drift was still less. The photocell drift for intermediate range may still be enough to vary its output. Considering the small distance between the fotonic sensor and the transducer membrane, one could easily discard any possibilities of light cancellation causing the drift.

All attempts to make average dc measurements of the sensor output following an equilibrium pressure level adjustment were unsuccessful. As a result, the transducer capability was demonstrated by its transient response to input pressure variations. Figure 16 shows such response which is at the same time the response to an approximate ramp function. Following this procedure, two sets of experiments were conducted. The first set of experiments studied the response of the transducer in the region of interest. The second series of tests were for pressures varying up to ten times the range of the first series in order to examine the linear response of the membrane.

Dynamic tests were conducted on the transducer by varying the input

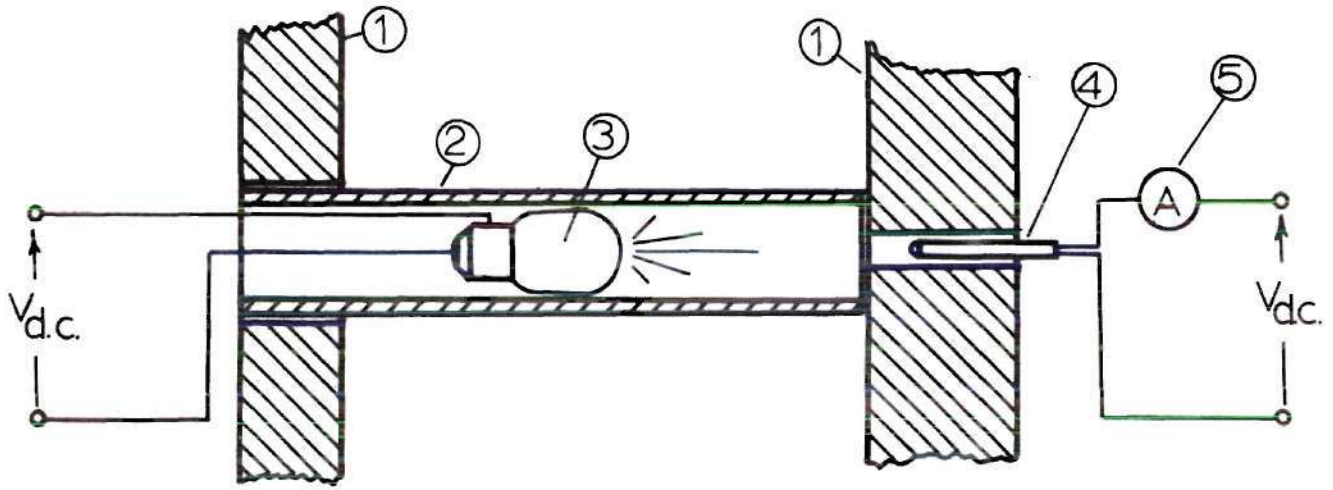


① Wooden blocks
② Cooper tube
③ Light bulb
④ Photocell
⑤ Picoammeter

Figure 15. Photocell Test Sketch

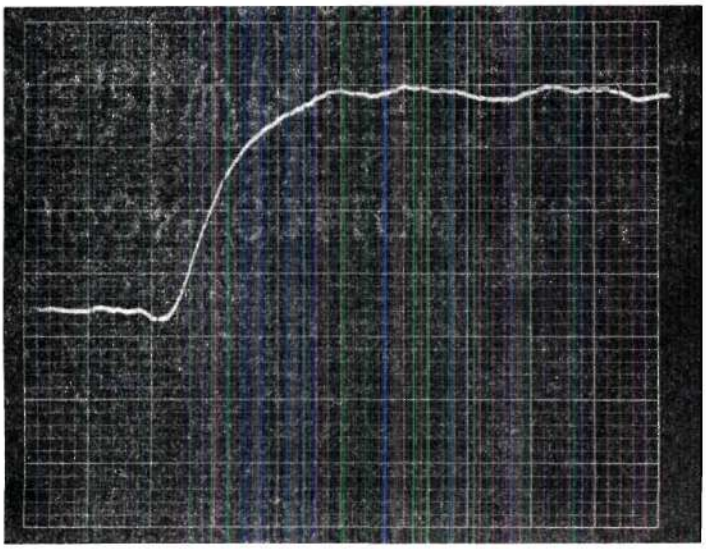

Figure 16. Typical Transient Response to a Ramp Input

signal frequency and recording the frequency response through the use of the test arrangement discussed earlier. Lissajous figures of the response were also obtained. These figures gave both the magnitude ratio and the phase shift. A typical response is sketched in Figure 17(a) and the actual photograph is shown in Figure 17(b). Gains and phase shifts were measured for various frequencies.

As pointed out earlier, the frequency response of the entire system included the characteristics of the pneumatic signal generator, connecting line dynamics, the Pitran transducer, the transducer under investigation, and the filter. The filter response was calculated by knowing the values of its components. The frequency responses of the pneumatic signal generator and the connecting line were obtained experimentally through the use of the Pitran transducer. Since the Pitran transducer had a flat frequency response up to one megaHertz, and since the upper limit of frequency for the transducer under investigation was only 60 Hertz, the Pitran output only appeared as a scalar multiple of the combined output of pneumatic signal generator and line dynamics. Having had the Pitran characteristics available (1.647 Volts/psi), the transfer function of the signal generator-line dynamics combination was determined.

In a very similar fashion, the fotonic sensor also acted as a pure scalar multiplier of the transducer output. This was due to the fact that the fotonic sensor had a flat frequency response up to 50 kiloHertz and the upper limit of frequency of interest in testing the transducer was only 60 Hertz.

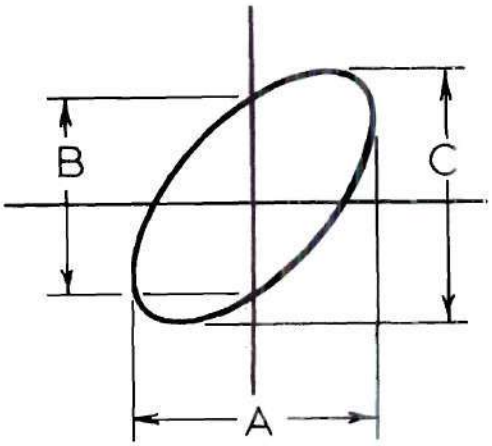


$$\text{GAIN} = \frac{C}{A}$$

$$\text{PHASE ANGLE} = \sin^{-1}\frac{A}{B}$$

(a) Lissajous figure

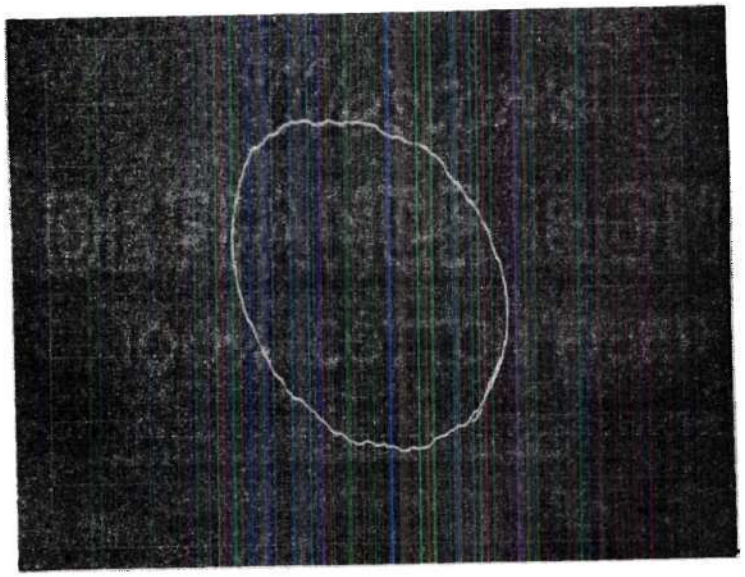

(b) transducer's Lissajous figure

Figure 17. Lissajous Figures Dynamic Response

The frequency response of the transducer under study was computed from the data for the individual components excluding the test unit in conjunction with the overall response of the open loop system shown in the block diagram of Figure 12(a).

# CHAPTER IV

## PRESENTATION AND DISCUSSION OF RESULTS

### Computation Procedure for Static Characteristics

The static characteristics of the transducer relate the output voltage change of the fotonic sensor as a function of the pressure change imposed on the transducer membrane. In order to obtain the true test pressure level in the transducer it was necessary to use an iteration procedure. This procedure allowed for the change in pressure of the cavity due to the membrane displacement. A simple block diagram of the iteration procedure is shown in Figure 18.

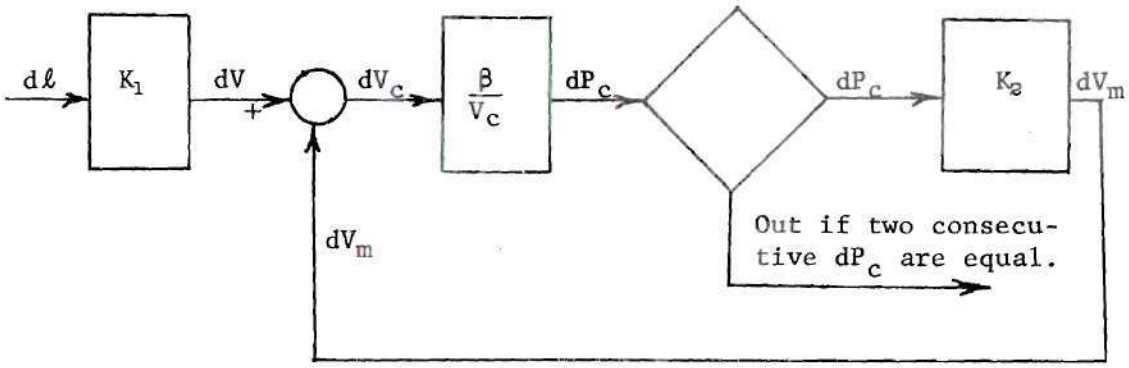


Figure 18. Static Computation Block Diagram

In this procedure a change in cavity volume corresponding to a change in piston displacement was computed. This was given by equation

$$dV = (0.785)\ d\ell = K_1\, d\ell,\ in^3 \tag{50}$$

The change in pressure corresponding to this change in volume was computed from

$$dP_c = \beta \frac{dV_c}{V_c} . \tag{51}$$

The maximum deflection of the diaphragm and the volume swept by the diaphragm due to the change in pressure was computed from

$$dV_m = \frac{(m^2-1)\ \pi\ r_o^6}{16R\ m^2 t^3}\ dP_c = K_2\, dP_c . \tag{52}$$

The above change in volume was compared with that obtained by equation (50) in the first step. The procedure was continued until the difference in pressure change calculated in one step and the next is very small (less than $\times\ 10^{-6}$ psi). That pressure is the actual system pressure.

The next item concerned itself with relating the change in output voltage to the change in calculated pressure. The bulk modulus of air for the isothermal process is related to pressure by

$$\beta = \bar{\bar{P}} . \tag{53}$$

The theoretical deflection of the membrane was calculated for the corrected pressure from a given piston displacement by

$$dy_{max} = \frac{(m^2-1)\ 3r_o^4}{16E\ m^2 t^3}\ dP . \tag{54}$$

The change in output voltage of the fotonic sensor was computed for the calculated deflection by

$$dE = (0.274)\ dy_{max} \quad . \tag{55}$$

This change in voltage was compared to the measured value from the tests. Table 1 shows the results of the iteration procedure. Table 2 shows the comparison between theoretical and experimental values of output voltages. The range of pressures used in these experiments was from atmospheric up to 0.012 pound per square inch. Similar computations and tests carried out for pressures up to ten times the values used in the preceding tests are shown in Table 3. These tests were conducted, as was pointed out earlier, specifically to examine the linear range of deflection of the membrane.

## Static Characteristics

The results of Table 2 are shown on the graph in Figure 19. Figures 20 and 21 show the experimental static characteristics of the transducer. It is seen from Table 3 that an essentially constant correction factor needs to be applied to the theoretical results in order to obtain a good comparison between theory and experiment. It is felt that the source of the error may be traced to the deformation of sealing rings which clamp the Mylar membrane. It is worth noting that theoretical results consistently yield a larger deflection of the membrane as compared to experimental values. It is also noted that the correction factor is different for two different series of tests with an intermediate readjust-

Table 1. Iterative Calculations for Pressure

| Piston Displacement $\times 10^{-4}$, in | Change of Volume Due to Piston $\times 10^{-4}$, $in^3$ | Change of Pressure $\times 10^{-3}$, psi | Change of Volume Due to Membrane $\times 10^{-6}$, $in^3$ | Corrected Change of Pressure $\times 10^{-3}$, psi |
|---|---|---|---|---|
| 8 | 6.28 | 1.415 | 3.9 | 1.406 |
| | | | 3.9 | 1.406 |
| 11 | 8.63 | 1.945 | 5.4 | 1.933 |
| | | | 5.4 | 1.933 |
| 12 | 9.42 | 2.122 | 5.9 | 2.109 |
| | | | 5.9 | 2.109 |
| 22 | 17.27 | 3.891 | 10.8 | 3.866 |
| | | | 10.8 | 3.866 |
| 14 | 10.99 | 2.476 | 6.9 | 2.460 |
| | | | 6.8 | 2.460 |

Table 2. Relationship of Experimental and Theoretical Change of Voltage

| Experimental | | Theoretical | | |
|---|---|---|---|---|
| Pressure $P$ $\times 10^{-3}$, psi | Voltage $E$ $\times 10^{-3}$, Volts | Deflection $y$ $\times 10^{-3}$, in. | Voltage $E$ $\times 10^{-3}$, Volts | $E_{exp}/E_{theo}$ |
| 0.0 | 0.0 | 0.0 | 0.0 | 0.0 |
| 1.40 | 3.2 | 0.24 | 65.8 | 0.048 |
| 3.33 | 5.2 | 0.57 | 156.3 | 0.033 |
| 5.44 | 7.2 | 0.93 | 255.0 | 0.028 |
| 9.31 | 11.4 | 1.59 | 436.1 | 0.026 |
| 11.77 | 16.6 | 2.01 | 551.3 | 0.030 |

Table 3. Relationship of Experimental and Theoretical Change of Voltage for Higher Pressure Range

| Experimental | | Theoretical | | |
|---|---|---|---|---|
| Pressure $P \times 10^{-3}$, psi | Voltage $E \times 10^{-3}$, Volts | Deflection $y \times 10^{-3}$, in. | Voltage $E \times 10^{-3}$, Volts | $E_{exp}/E_{theo}$ |
| 0.0 | 0 | 0.0 | 0.0 | 0.0 |
| 1.93 | 3 | 0.32 | 90.0 | 0.033 |
| 7.90 | 12 | 1.34 | 368.2 | 0.032 |
| 14.58 | 18 | 2.48 | 679.2 | 0.026 |
| 19.15 | 25 | 3.25 | 892.0 | 0.028 |
| 20.91 | 29 | 3.55 | 973.8 | 0.029 |
| 27.06 | 36 | 4.60 | 1260.2 | 0.028 |
| 32.51 | 43 | 5.53 | 1513.9 | 0.028 |
| 39.00 | 53 | 6.63 | 1816.1 | 0.029 |
| 44.63 | 61 | 7.59 | 2078.0 | 0.029 |
| 55.70 | 78 | 9.47 | 2593.6 | 0.030 |
| 64.14 | 90 | 10.90 | 2986.4 | 0.030 |
| 75.56 | 110 | 12.85 | 3518.4 | 0.031 |
| 88.92 | 129 | 15.12 | 4140.3 | 0.031 |
| 95.60 | 142 | 16.26 | 4451.3 | 0.031 |
| 101.75 | 153 | 17.30 | 4737.7 | 0.029 |
| 109.84 | 165 | 18.68 | 5114.2 | 0.034 |

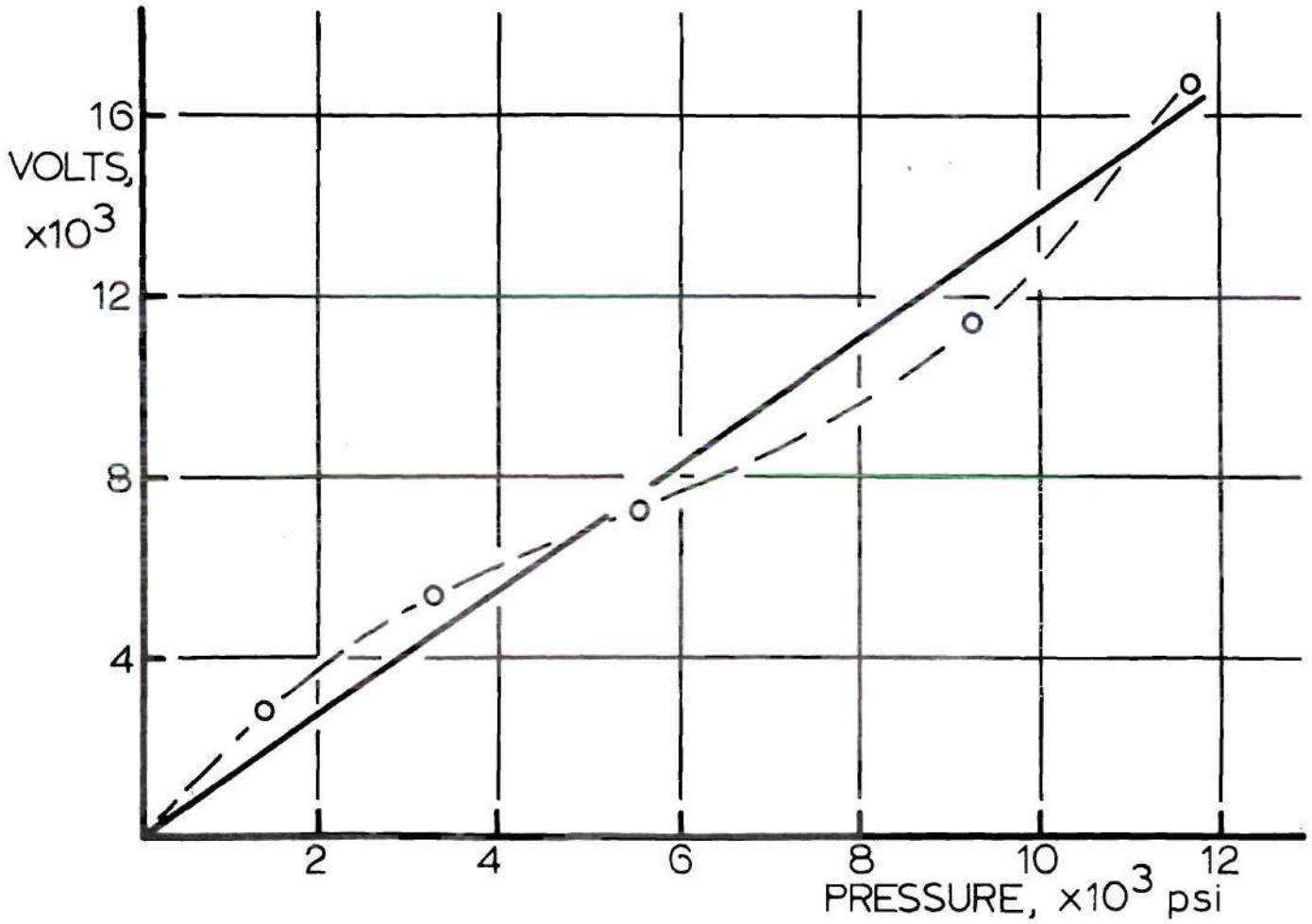


Figure 19. Static Characteristic for Low Pressure

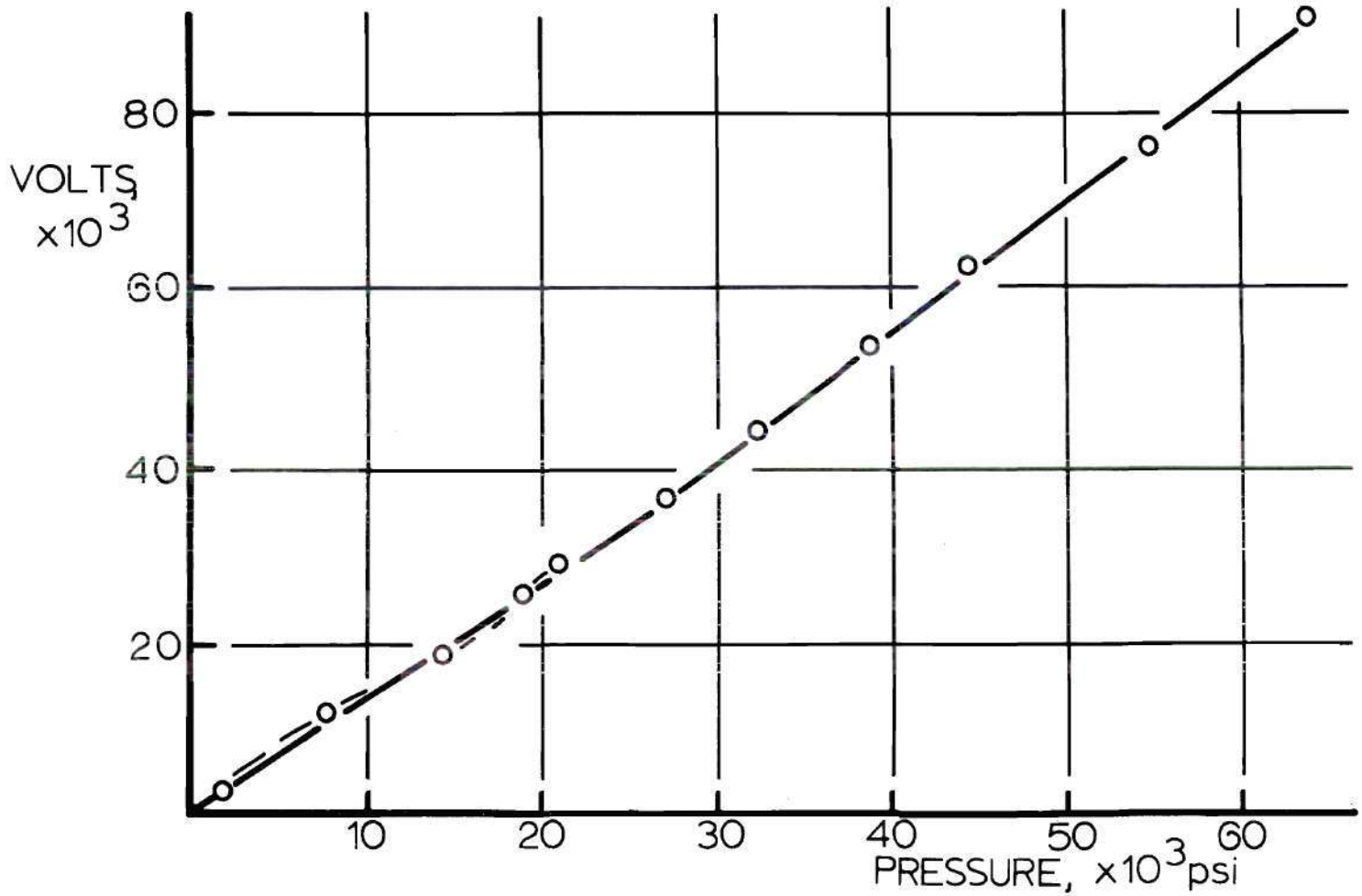


Figure 20. Static Characteristic for Medium Pressure Range

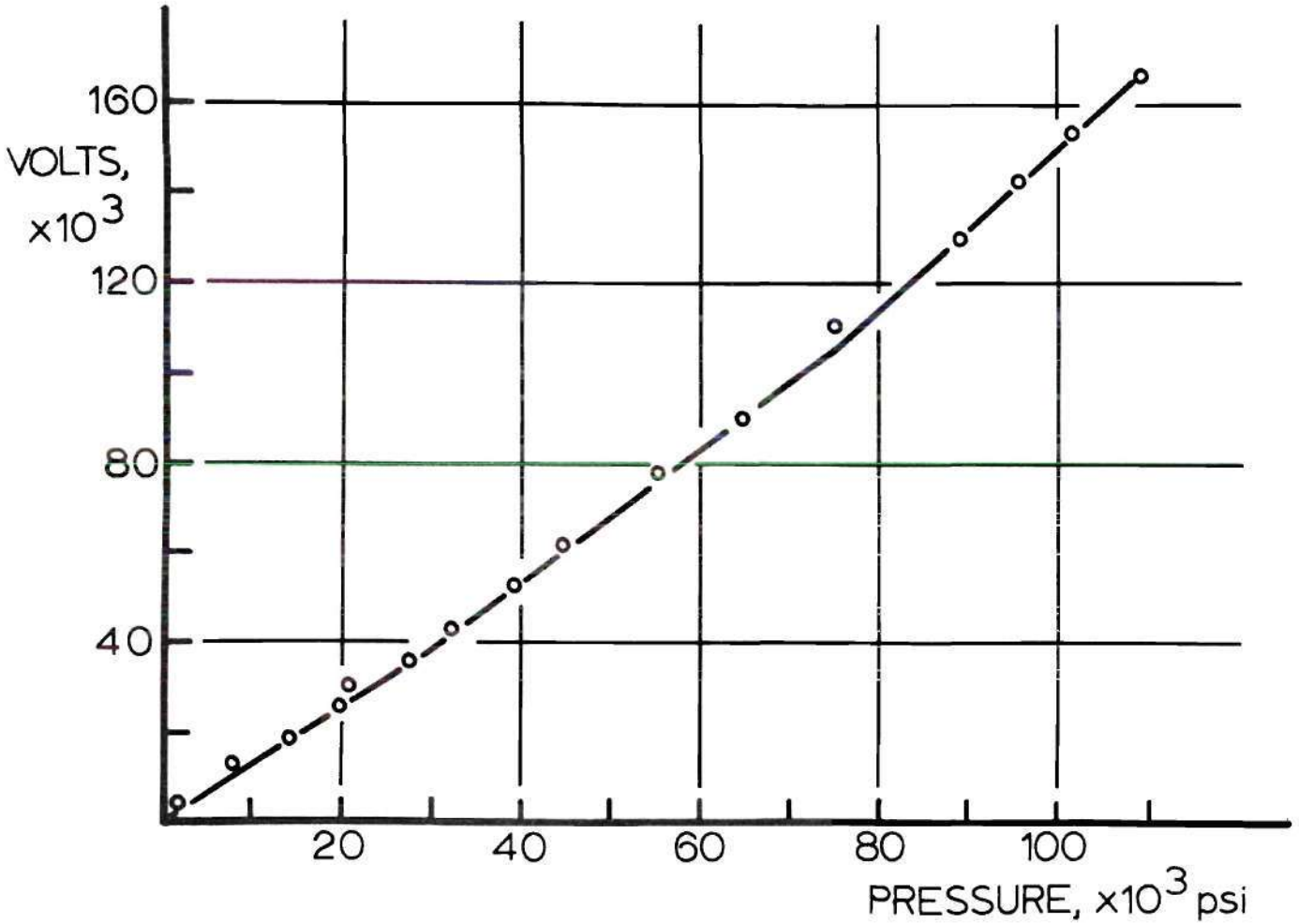


Figure 21. Static Characteristic for Higher Pressure Range

ment of the membrane clamped by sealing rings. As a result it is likely that the effective diameter of the membrane was reduced from its nominal size as a function of excessive tightening and resulting deformation of the sealing rings. On the other hand, it is recognized that the use of sealing rings in properly clamping the membrane is necessary to avoid leakage. It is also recognized that, due to the ductile nature of Mylar membrane, it is particularly cumbersome to seal the system. Figures 19 and 20 show that in the range of pressures of interest the transducer characteristics are not linear. Figure 21 shows that the behavior becomes linear only after the application of a certain level of pressure. It may be noted that a linear relationship exists for a low pressure range (0.027 to 0.076 psi), and another linear relationship with a different slope exists for the next higher pressure range (higher than 0.076 psi). This behavior, however, can easily be accommodated for in the static calibration curve of the device.

Figure 22 shows a comparison of the experimental results with the modified theoretical results, where the latter are multiplied by a constant factor of 0.033 for the low pressure range. Figure 23 shows similar comparison for higher pressure range (0 to 0.1098 psi), the correction factor applied to the theoretical results being 0.0302.

It is noted that there is a good agreement between the experimental and analytical static characteristics for pressures above 0.076 psi with an error of less than seven percent.

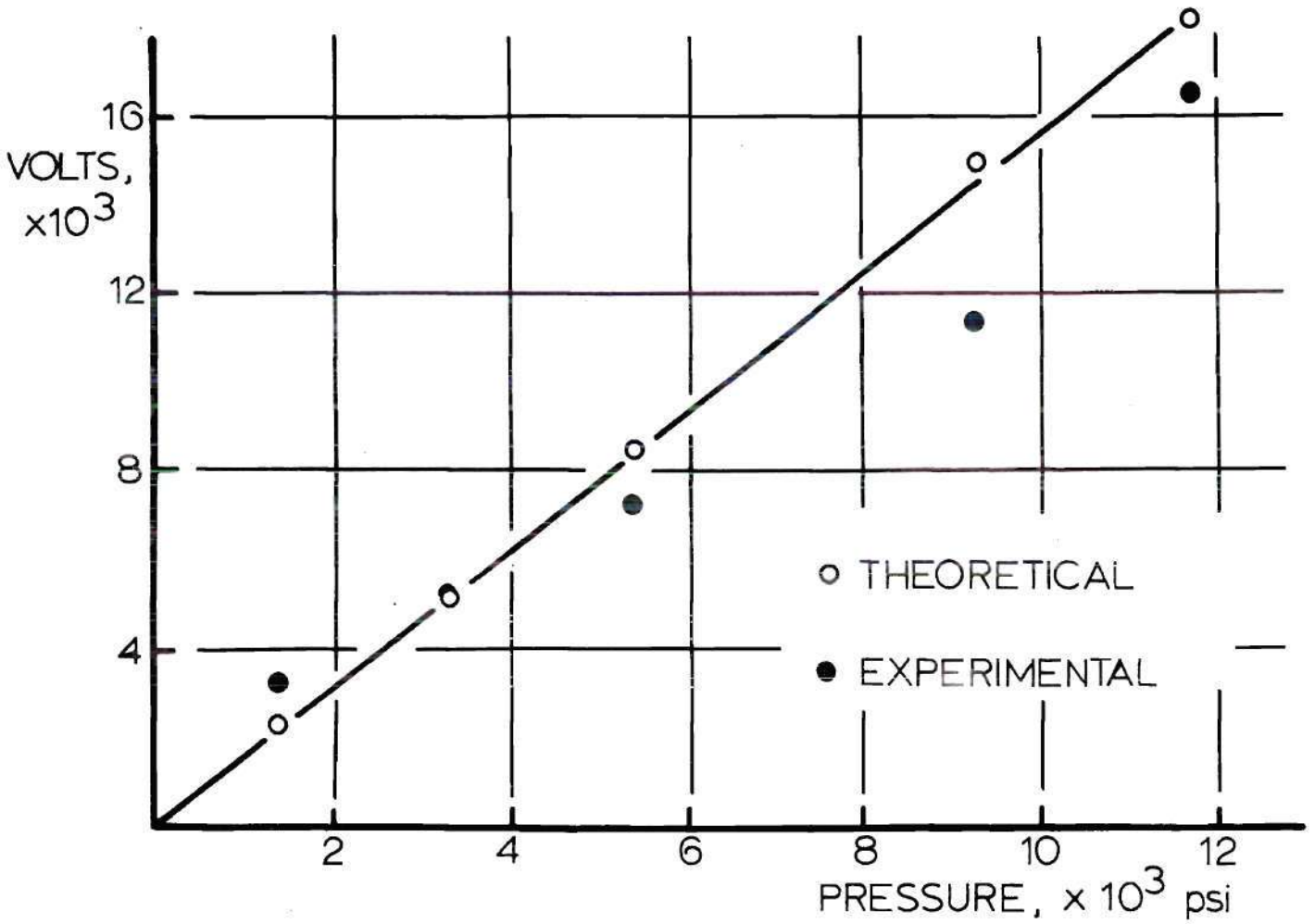


Figure 22. Comparison of Experimental and Theoretical Voltage

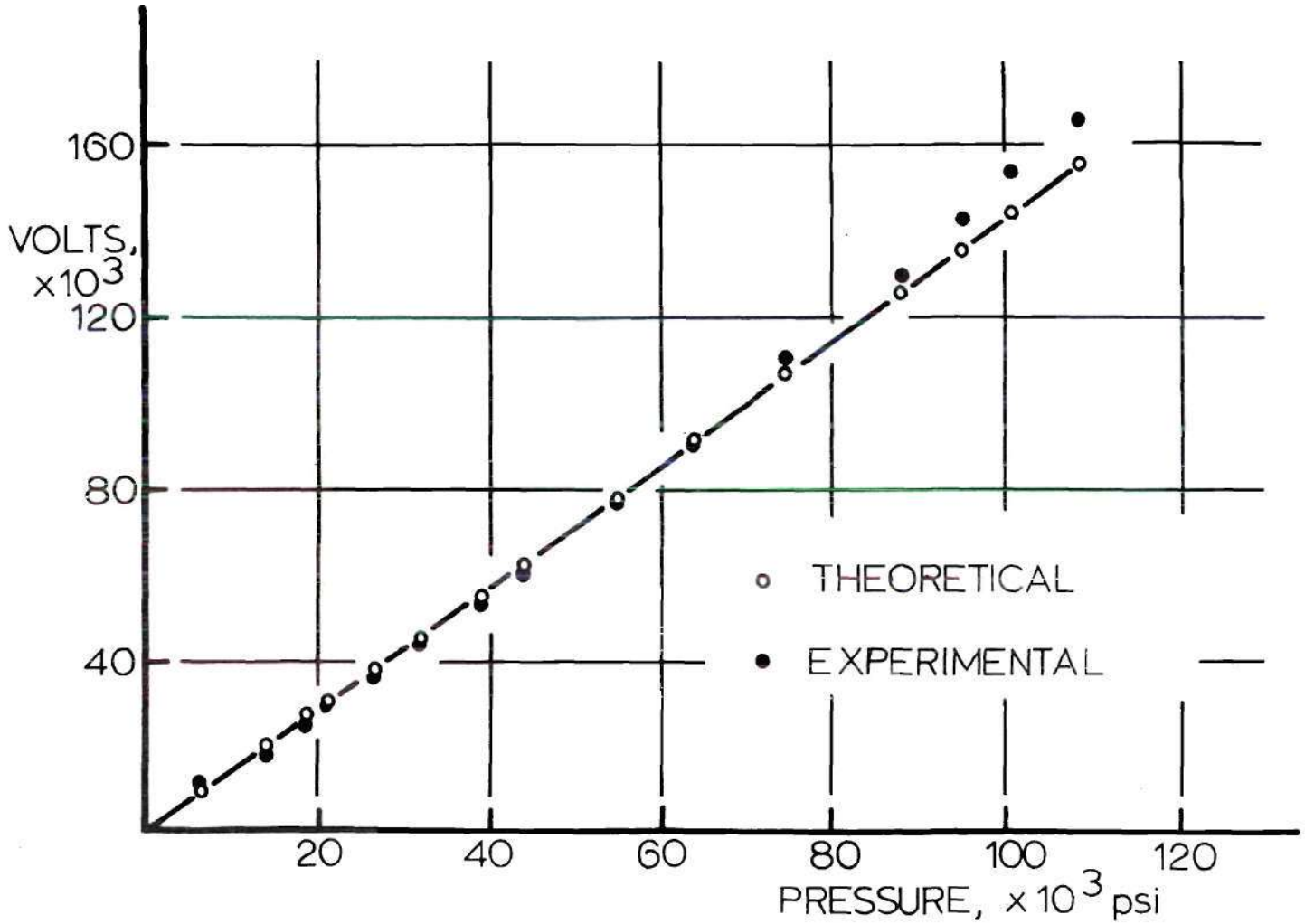


Figure 23. Comparison of Experimental and Theoretical Voltage for Higher Pressure Range

## Computation of Dynamic Characteristics

It was discussed earlier in Chapter III that the frequency response of the test-transducer was computed by first obtaining the individual frequency responses of all the system components, excluding the test unit and then obtaining the data for the total system, including the test unit.

The frequency response data for the filter were computed from the equation given in Figure 14 with R = 1,000 ohms and C = 2,000 microfarads, which is shown in Table 4. The frequency response test data for the pressure signal generator and the transmission line are shown in the second and third columns of Table 5. The frequency response data for the entire system including the test-transducer are shown in the fourth and fifth columns of Table 5. The fotonic sensor characteristics can be obtained from static tests as 1.76 Volts per psi, which represents a gain that can be expressed as 4.75 db.

The frequency response of the test-transducer can now be computed as the difference in magnitude and phase shift in a logarithmic plot of the data of the total system and the data for each individual component. For a given frequency, the magnitude of the filter shown in Table 4, the magnitude of the pressure signal generator shown in the second column of Table 5, and the gain of the fotonic sensor, each, was subtracted from the magnitude of the entire system shown in the fourth column of Table 5. A similar procedure is applied to the computation of phase shift. The frequency response for the transducer thus obtained is shown in Table 6, and is shown plotted in Figure 24.

Table 4. Frequency Response of Filter

| Frequency Cycles per Second | Gain Decibels | Phase Angle Degrees |
|---|---|---|
| 5 | - 20.04 | - 84.3 |
| 6 | - 21.61 | - 85.3 |
| 7 | - 22.94 | - 86.0 |
| 8 | - 24.09 | - 86.5 |
| 9 | - 25.11 | - 86.9 |
| 10 | - 26.03 | - 87.2 |
| 15 | - 29.54 | - 88.1 |
| 20 | - 32.04 | - 88.6 |
| 25 | - 33.97 | - 88.9 |
| 30 | - 35.56 | - 89.0 |
| 35 | - 36.89 | - 89.2 |
| 40 | - 38.06 | - 89.3 |
| 45 | - 38.99 | - 39.4 |
| 50 | - 40.00 | - 89.45 |
| 60 | - 41.58 | - 89.5 |

Table 5. Experimental Frequency Response for the Entire System and Pressure Signal Generator-Line Dynamics

| Frequency Cycles per Second | Pressure Signal Generator-Line Dynamics | | Entire System | |
|---|---|---|---|---|
| | Gain Decibels | Phase Angle Degrees | Gain Decibels | Phase Angle Degrees |
| 5 | - 5.09 | - 25 | - 43.87 | - 104.7 |
| 6 | - 5.49 | - 28.1 | - 44.94 | - 107.2 |
| 7 | - 5.71 | - 30.0 | - 46.13 | - 122.0 |
| 8 | - 5.42 | - 37.8 | - 46.24 | - 113.0 |
| 9 | 5.71 | - 40.2 | - 48.51 | - 120.0 |
| 10 | - 5.76 | - 44.4 | - 48.51 | - 118.0 |
| 15 | - 6.91 | - 51.15 | - 55.24 | - 131.5 |
| 20 | - 8.18 | - 65.5 | - 60.42 | - 149.0 |
| 25 | - 9.24 | - 75.2 | - 64.49 | - 156.0 |
| 30 | - 11.08 | - 84.6 | - 64.37 | - 165.4 |
| 35 | - 12.06 | - 93.1 | - 66.84 | - 165.4 |
| 40 | - 13.04 | - 101.6 | - 68.24 | - 165.6 |
| 45 | - 13.92 | - 112.2 | - 70.62 | - 179.5 |
| 50 | - 15.08 | - 116.5 | - 72.53 | - 195.4 |
| 60 | - 16.87 | - 121.4 | - 73.45 | - 203.6 |

Table 6. Transducer Frequency Response

| Frequency Cycles per Second | Gain Decibels | Phase Angle Degrees |
|---|---|---|
| 5 | - 14.93 | - 0.40 |
| 6 | - 14.03 | + 6.20 |
| 7 | - 13.49 | - 6.00 |
| 8 | - 12.51 | + 11.30 |
| 9 | - 13.88 | + 7.10 |
| 10 | - 12.32 | + 13.60 |
| 15 | - 14.96 | + 7.75 |
| 20 | - 16.38 | + 5.10 |
| 25 | - 17.46 | + 8.10 |
| 30 | - 14.91 | + 8.20 |
| 35 | - 14.07 | + 16.90 |
| 40 | - 13.32 | + 24.30 |
| 45 | - 13.89 | + 22.10 |
| 50 | - 13.74 | + 10.50 |
| 60 | - 11.17 | + 7.30 |

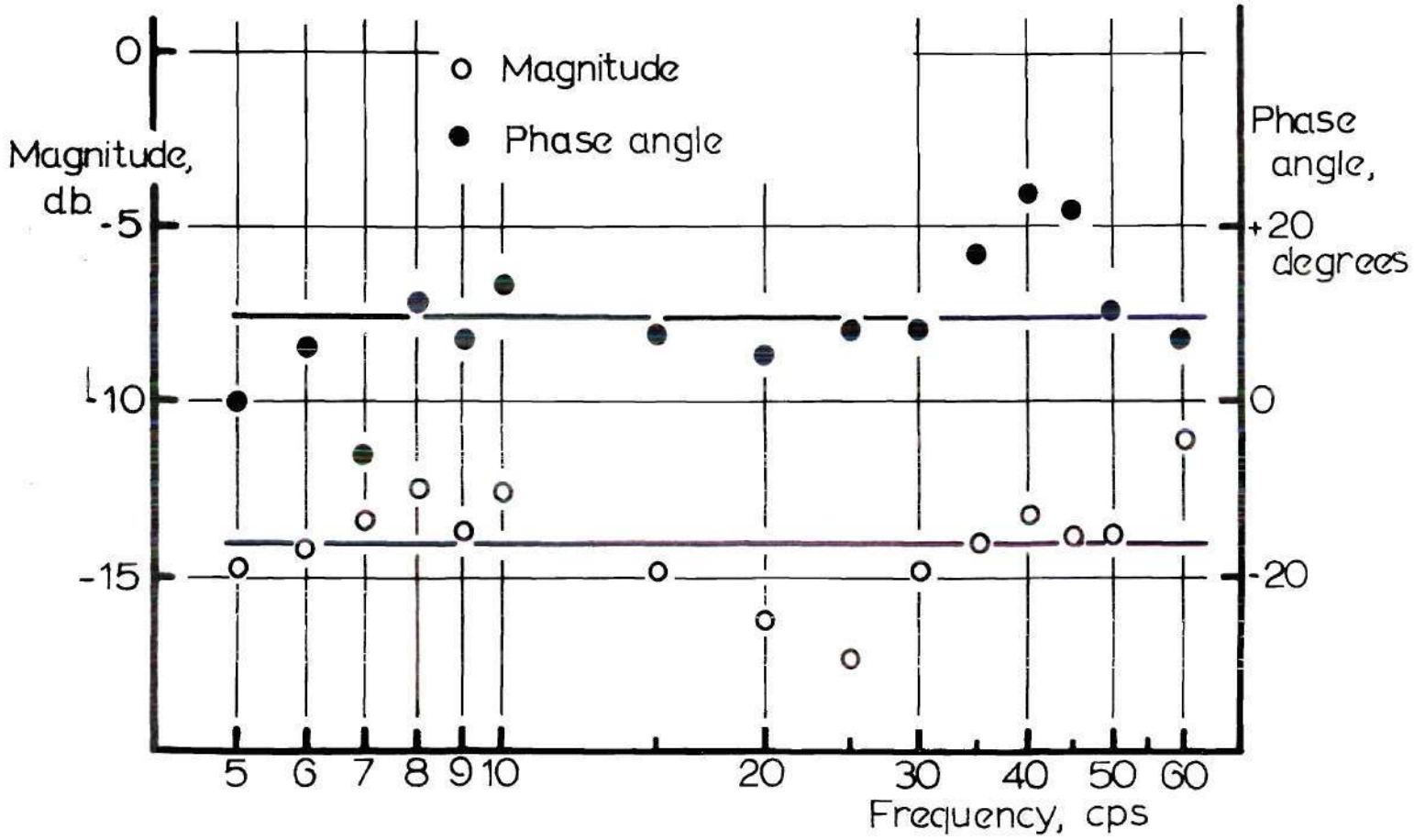


Figure 24. Experimental Frequency Response of Transducer

## Dynamic Characteristics

Figure 24 shows the frequency response of the low pressure transducer under investigation. A straight line approximation may be fitted to all these data points. Such an approximation is drawn by neglecting two extreme data points to yield a first order response and by taking an average of the remaining points. The error of the data points compared to the straight line approximation goes from 11 percent for the lower extreme case to 16.6 percent for the upper one. The gain of the transducer is -14.05 db, which implies a 50 percent loss. Considering the experimental nature of the determination of the response obtained from Lissajous figure photographs, the errors are to be expected. The phase angle, as determined by a similar procedure, is 8.2 degrees. Again, the technique using experimental Lissajous figures is responsible for the positive phase shift, instead of a phase lag.

The Pitran and fotonic sensor frequency responses were considered flat which is valid only for a variation of plus or minus 3 db. This, in the worst of the cases, makes a six db difference in the magnitude ratio which could lower the average value of gain from -14 db to -8 db.

It is interesting to observe that the dynamic characteristics show considerable losses which were neglected in the analytical predictions. On the other hand, it is seen that the frequency response is flat, without a phase shift variation with frequency, up to a frequency of 60 Hertz. This result is consistent to a certain extent with analytical predictions.

# CHAPTER V

# CONCLUSIONS AND RECOMMENDATIONS

## Conclusions

This investigation of the analysis, design, fabrication, and testing of a low pressure transducer has led to the following conclusions:

1. The concept, utilizing an optical proximity sensor and the deflection of a very thin Mylar membrane, is a fruitful one leading to a feasible configuration for a low pressure transducer. It might be interesting to note that the Mosaic Division of Bendix Corporation has recently announced a pressure transducer operating on a similar concept, the basic difference being their use of reflected intensity from a membrane rather than the proximity used in the present investigation.

2. The response of the transducer is quite linear over a wide range of pressures up to the yield point of the membrane material as well as within the linear range of operation of the fotonic sensor.

3. A transducer with a membrane made of plastic material is not very suitable for very small deformations because it is not linear. However, the performance improves significantly for bigger deformations which yield linear responses.

4. An increase in the diameter of the membrane results in an increase in deformation for the same input pressure, which points to a more effective use of the linear range of the deformation curve.

5. The transducer can be used for absolute and differential pressure measurements applications, involving both static and dynamic pressures. A set of different membrane materials or different thicknesses of the same material may be used for very wide ranges in pressure. The transducer can be used over the second linear region of the characteristic curve of the fotonic sensor for measurements of relatively large deflections of the membrane.

6. Both sides of the membrane must be at the same temperature, otherwise a change of pressure is noticeable.

7. The frequency response of the transducer is flat and with zero phase shift up to a frequency of 60 cycles per second. The analytical model neglecting the line volume predicts quite realistic results for the dynamic response of the transducer if attention is paid to mechanical losses.

## Recommendations

On the basis of the experience gained during this investigation, the following recommendations are made for further effort on this research project:

1. It is recommended that, instead of using the power supply of the fotonic sensor, a dry cell battery with the same voltage be used in order to assure relatively noise-free supply voltage.

2. For phase shift measurements, use of a phase shift device together with the Lissajous figures is recommended, instead of using only the latter.

3. A design configuration allowing for a more flexible holding mechanism with the capability of holding different diameter membranes needs to be investigated.

4. A design consisting of a transparent transducer main body is recommended, so that the position of the fotonic sensor with respect to the membrane may be directly observed. A built in fiber optics in the transducer assembly may be more convenient from the viewpoint of repairing leakage problems. It is suggested that such a design be considered.

5. The use of a smaller piston and a bigger volume for more sensitivity is definitely recommended if the present scheme of reference pressure is to be followed.

# BIBLIOGRAPHY


1. Roark, R. J., "Formulas for Stress and Strain," first ed., McGraw-Hill Book Company, New York, 1938, p. 170.

2. Miles, D. O., "Direct Mechanical Determination of the Dynamic Response of Diaphragms," J. of the Acoustical Soc. of America, Vol 36, no. 9, August 1964, pp. 1471-78.

3. Modern Plastic Encyclopedia; Bresklin and Charlton Publishing Corporation, New York, 1962, p. 20.

4. Harrison, H. L., and Bollinger, J. G., "Introduction to Automatic Controls," 2nd ed., International Textbook Company, Pennsylvania, 1969, p. 188.

5. Schuder, C. B., and Binder, R. C., "The Response of Pneumatic Transmission Lines to Step Inputs," Trans. ASME, Series D, J. of Basic Eng., Vol 81, December 1958, pp. 578-584.

6. Doebelin, Ernest O., "Measuring Systems: Application and Design," New York, McGraw Hill, 1966.

7. Hollman, J. P., "Experimental Methods for Engineers," McGraw-Hill, 1966.

8. Brown, F. T., "The Transient Response of Fluid Lines," Trans. ASME, Series D, J. of Basic Eng., Vol 89, no. 2, June 1967, pp. 547-553.

9. Karam, J. T., and Franke, M. E., "The Frequency Response of Pneumatic Lines," Trans. ASME, Series D, J. of Basic Eng., Vol 89, no. 2, June 1967, pp. 371-378.

10. Daily, J. W., and Harleman, D. R. F., "Fluid Dynamics," Addison-Wesley Publishing Company, Inc., 1967.

11. Takahashi, Y., Rabins, M. J., and Auslander, D. M., "Control," Addison-Wesley Publishing Co., Inc., 1970.